How can we understand the global distribution of the solar cycle signal on the Earth's surface?

Kunihiko Kodera[1], Rémi Thiéblemont[2], Seiji Yukimoto[3], Katja Matthes[4,5]

[1]Institute for Space-Earth Environmental Research, Nagoya University, Nagoya, 464-8601 Japan
[2]Laboratoire Atmosphères Milieux Observations Spatiales, Guyancourt, 78280, France
[3]Meteorological Research Institute, Tsukuba, 305-0052 Japan
[4]Research Division Ocean Circulation and Climate, GEOMAR Helmholtz Centre for Ocean Research, Kiel, 24105 Germany
[5]Christian-Albrechts Universität zu Kiel, Kiel, 24105 Germany

Correspondence to: Kunihiko Kodera (kodera@isee.nagoya-u.ac.jp)

Abstract. To understand solar cycle signals on the Earth's surface and identify the physical mechanisms responsible, surface temperature variations from observations as well as climate model data are analyzed to characterize their spatial structure. The solar signal in the annual mean surface temperature is characterized by i) mid-latitude warming and ii) no overall tropical warming. The mid-latitude warming during solar maxima in both hemispheres is associated with a downward penetration of zonal mean zonal wind anomalies from the upper stratosphere during late winter. During Northern Hemisphere winter this is manifested in a modulation of the polar-night jet whereas in the Southern Hemisphere the subtropical jet plays the major role. Warming signals are particularly apparent over the Eurasian continent and ocean frontal zones, including a previously reported lagged response over the North Atlantic. In the tropics, local warming occurs over the Indian and central Pacific oceans during high solar activity. However, this warming is counter balanced by cooling over the cold tongue sectors in the southeastern Pacific and the South Atlantic, and results in a very weak zonally averaged tropical mean signal. The cooling in the ocean basins is associated with stronger cross-equatorial winds resulting from a northward shift of the ascending branch of the Hadley circulation during solar maxima. To understand the complex processes involved in the solar signal transfer, results of an idealized middle atmosphere–ocean coupled model experiment on the impact of stratospheric zonal wind changes are compared with solar signals in observations.

Although the momentum forcing differs from that of solar radiative forcing, the model results suggest that stratospheric changes can influence the troposphere not only in the extra-tropics but also in the tropics through i) a downward migration of wave–zonal mean flow interactions and ii) changes in the stratospheric mean meridional circulation. These experiments support earlier evidence of an indirect solar influence from the stratosphere.

1 Introduction

The influence of solar activity on the Earth's surface, especially that of the 11-year solar cycle, has been debated for a long time (e.g., Pittock, 1978; Legras, 2010). The climate impact of solar influence is generally assessed in terms of the radiative

forcing (e.g., IPCC, 2013). Recent direct measurements from space reveal that changes in the total solar irradiance (TSI) associated with the 11-year solar cycle are about 0.1% (1.3 W m^{-2}) (Kopp and Lean, 2011). Such small variations are not expected to have a significant impact on surface climate, and so several mechanisms have been proposed that act to amplify the initially small solar effects. One amplification mechanism is enhancement of the direct TSI effect at the ocean surface due to a feedback of water vapor transport in the tropical Pacific (Meehl et al., 2008, 2009). Another possible amplification mechanism works through a change in the solar spectrum, in particular in the ultra-violet (UV) range, directly affecting the stratopause region and enhancing temperatures and ozone concentrations during solar cycle. The amplification and the downward penetration of the small initial solar signal occur through stratospheric dynamical processes (e.g., Kodera and Kuroda, 2002). The impact of cosmic rays on surface temperature through changes in cloud cover has also been proposed (Svensmark and Friis-Christensen, 1997).

Besides apparently small direct solar effect, another problem of explaining solar influence on climate is the rather unstable relationship between the 11-year solar cycle and the Earth's global mean surface temperature, as a breakdown or even the reversal of the relationship occurs during different time periods (e.g., Nitta and Yoshimura, 1993; Georgieva et al., 2007; Souza-Echer, 2012). However, Zhou and Tung (2010) extracted a global spatial pattern of sea surface temperature (SST) variations associated with the solar cycle by applying a composite mean difference (CMD) projection method; i.e., taking the composite difference between periods of high and low solar activity during the 11-year cycle. They demonstrated that the coefficients of this CMD pattern projected onto the global SST field show a steady and highly robust relationship with the solar activity more than 10 solar cycles (represented by the TSI for the past 153 years reconstructed by Wang et al., 2005). This indicates that a global spatial pattern, rather than a globally averaged quantity, is crucial to understanding solar influences at the surface.

Various studies of the solar influence on weather and climate were reviewed by Gray et al. (2010). Here, we do not attempt to extensively review previous works, but rather find consistent aspects of the solar signals reported in many independent studies. It should be noted that most of the previous work investigated processes producing solar signals on the Earth's surface in a specific region. Little was done to understand the overall aspect of solar signals on the entire Earth's surface.

Surface temperature and pressure have been measured for more than 100 years. Thus, the relationship between surface temperature variations and solar activity can be investigated using a global historical dataset. Because sea surface temperature (SST) is more persistent than the sea-level pressure (SLP), long-term variations can be more easily detected in the temperature field. Therefore, we investigate mainly surface temperature variation from the historical data, complimented by pressure or geopotential height fields with a modern dataset.

Annual mean surface temperature anomalies related to the solar cycle have been studied using various methods and different historical global datasets covering between 120 and 150 years. Lohmann et al. (2004) calculated the correlation coefficient between the proxy solar irradiance from Lean et al. (1995) and band-pass (9−5 year period) filtered SSTs reconstructed by Kaplan et al. (1998) from 1856 to 2000. Lean and Rind (2008) extracted solar signals by applying a multiple linear regression analysis to surface temperatures reconstructed by the University of East Anglia Climatic Research Unit F (Brohan et al., 2006) for the period 1889–2006. A similar multiple linear regression analysis was conducted by Tung and Zhou (2010), who compared the regression analysis of two different historical datasets, namely NOAA's Extended Reconstructed Sea Surface Temperatures (ERSST) and the Hadley Centre Sea Ice and Sea Surface Temperature (HadISST) dataset (Rayner et al., 2003), to confirm consistent features of the solar signal. Gray et al. (2013) performed a lagged multiple linear regression analysis to investigate delayed components in the solar signal using the HadISST dataset. Despite different reconstructions and analysis methods, common features are seen during high solar activity in the surface temperatures: a mid-latitude warming, and a tropical cooling in the southeastern Pacific and the South Atlantic. Note that this cooling is different from the La Niña-like pattern previously reported (van Loon et al., 2007; Meehl et al., 2008, 2009) and will be discussed in more detail below.

We first compare the analysis results of a historical surface temperature dataset with those of a modern dataset to identify the fundamental global features of surface temperature variations related to the solar cycle; i.e., the observed solar surface signal. Next, we study the vertical structure of the solar signal with recent data to identify the physical mechanisms producing the solar surface signals. Identification of the causes and characteristics of solar signals is particularly difficult for decadal-scale periodic variations because strong feedbacks exist on these timescales in the climate system. To better understand the mechanisms producing a solar surface signal, we revisit results from an idealized middle atmosphere–ocean coupled general circulation experiment where a momentum forcing has been applied in the stratosphere (Yukimoto and Kodera, 2007).

The remainder of this paper is organized as follows. After a brief explanation of the data and method of analysis in section 2, characteristics of the solar signal in atmospheric as well as oceanic variables are described in section 3. To understand the complex processes for the solar signal transfer involving stratosphere–troposphere–ocean coupling, results of an idealized numerical experiment are compared with observed solar signals in section 4. To get insight into a centennial solar variation such as the Maunder minimum, the effect of centennial scale stratospheric circulation changes on the troposphere is briefly studied in section 5. Finally, a discussion and concluding remarks about the possible mechanisms producing the solar influence on the Earth's surface are given in section 5.

2 Data and Analysis

2.1 Data

This study combines the analysis of a historical SST dataset to characterize the surface response to the 11-year solar cycle, with a modern reanalysis dataset to investigate the underlying dynamical processes. For the historical dataset, we use the NOAA Extended Reconstructed SST v3b (ERSST), described by Smith et al. (2008) and available at http://www.esrl.noaa.gov/psd/data/gridded/data.noaa.ersst.html. The ERSST dataset spans more than 160 years from 1854 to the present, with monthly resolution, and a spatial resolution of 2° longitude × 2° latitude from 88°N to 88°S and 0°E to 358°E. Note that, however, data are sparse before 1880.

To examine the tropospheric and stratospheric dynamical response to the solar cycle, we use the ERA-Interim atmospheric reanalysis produced by the European Centre for Medium-Range Weather Forecasts (ECMWF) (Dee et al., 2011). The ERA-Interim (ERA-I) dataset is provided from 1 January 1979 to the present. In this study, we used monthly mean data, provided on 23 pressure levels from 1000 hPa to 1 hPa with a spatial resolution of 2.5° longitude × 2.5° latitude.

2.2 Multiple linear regression model

Following numerous earlier studies (e.g., Lean and Rind, 2008; Frame and Gray, 2010; Chiodo et al., 2014; Mitchell et al., 2015a,b), the ocean and atmosphere responses to solar variations are examined using a multiple linear regression model (MLR). This technique can isolate the effects of different forcings, represented by explanatory variables (or regressors), on the variance of a time-dependent variable (or predictand). Annual signals are extracted by applying the MLR to continuous monthly resolved time series. Monthly or seasonal signals (two to three consecutive months) are diagnosed by applying the MLR to time series of the individual month or season (i.e., the seasonal average is performed prior to the MLR), respectively. All data time series have the seasonal cycle removed before the MLR, as well as before any seasonal-average calculations. The MLR model is applied at each location and is given by

$$X(t) = A \cdot CO_2(t) + B \cdot N3.4(t) + C \cdot F10.7(t - \Delta t) + D \cdot AOD(t) + E \cdot QBOa(t) + F \cdot QBOb(t) + \epsilon(t), \quad (1)$$

where $X(t)$ is the time dependent variable, the first six terms on the right-hand side of the equation correspond to the product of one time-dependent explanatory variable (e.g., $CO_2(t)$) and its regression coefficient (e.g., A), and the last term $\varepsilon(t)$ is the residual error.

The explanatory variables considered for the MLR describe variability sources that are demonstrated to have a significant impact on the surface, troposphere and middle atmosphere dynamics and have been broadly used in solar-climate studies based on model and reanalysis (e.g. Chiodo et al., 2014 ; Mitchell et al., 2015a,b). The explanatory variables are defined as

follows: the CO_2 concentration (Meinshausen et al., 2011) (available at http://climate.uvic.ca/EMICAR5/forcing_data/RCP85_MIDYR_CONC.DAT) to account for the increase in anthropogenic forcing; the Nino 3.4 index derived from the ERSST v3b dataset; the F10.7 cm solar radio flux index (available at http://lasp.colorado.edu/lisird/tss/noaa_radio_flux.html); and the global aerosol optical depth (AOD) at 550 nm updated from Sato et al. (1993) to represent volcanic effects and two quasi-biennial oscillation (QBO) orthogonal indices (QBOa and QBOb) defined as the first two principal components of the ERA-I zonal mean zonal wind in the latitude interval (10°S, 10°N) and pressure–height interval (70− 5) hPa, respectively. Since the ERA-I dataset only starts in 1979, the QBO regressors are removed from the MLR when the long-term historical dataset (i.e., ERSST) is analyzed. Similarly, we used the solar sunspot numbers as regressor for the analysis of the ERSST dataset instead of the F10.7 index, which is not available before 1947. Note that to examine the stratospheric response to solar variations, the F10.7 cm index is more relevant than the sunspot number as it reproduces most of the variability of the UV band (Tapping, 2013). The solar regression coefficient used in our study assumes that a difference of 130 solar flux units (1 sfu = 10^{-22} W m^{-2} Hz^{-1}) or 100 sunspots represents the difference between the 11-year solar cycle maximum and minimum. To investigate the effect of the ocean memory on the surface response to solar variability (e.g., Gray et al., 2013; Thiéblemont et al., 2015), we calculated the MLR at different time lags (Δt in months or years) with respect to the solar regressor. The Arctic Oscillation (AO) or the North Atlantic Oscillation (NAO) is climate mode which is partly driven by solar variability as will be shown later. Hence, it is not relevant to include its index in a MLR model which aims at examining the solar cycle effect on surface climate.

When applying regression techniques, it is essential to carefully consider possible autocorrelation in the residual to assess statistical significances of the regression coefficients. Autocorrelation in the residual leads to an underestimation of the regression coefficient uncertainties, and thus a narrowing of the confidence intervals. A common method employed to circumvent the residual autocorrelation problem is to treat the residual term as an (first-order?) autoregressive process (Tiao et al., 1990). The first step of the procedure, also called prewhitening, consists of correcting both the predictors and the predictand (X) with the autocorrelation coefficient of the residual term estimated from a first application of the regression model. The prewhitening procedure is then repeated on the modified predictors and predictand until the residual is no longer significantly autocorrelated. The statistical significance of the autocorrelation is assessed with a Durbin–Watson test. The application of the Tiao et al. method can be found in several papers examining the solar signal (e.g., Austin et al., 2008 ; Mitchell et al., 2015b). We generally found that a single application of the prewhitening procedure was sufficient to remove the residual autocorrelation almost completely (more than 95% of the grid points). Once the prewhitening step has been performed, the statistical significance of the regression coefficients is calculated using a two-tailed Student's t-test.

The use of the MLR approach to separate the contribution of different factors on climate variability has inherent limitations that should be kept in mind when analyzing the results. The MLR particularly relies on several assumptions that may not be valid in all cases. However, composite analysis of the monthly mean data based on two or three levels of solar activity (e.g.,

Kuroda and Kodera, 2002; Lu et al., 2011) also produces similar solar signals as those obtained from the MLR method (Figs. 5, 6). Therefore, in spite of the limitations, the MLR method may be useful to get approximate solar signals (Kuchar et al., 2015). We note that highly non-linear responses can be produced through the interaction between different forcings: for example between ENSO and solar signals (Marsh and Garcia, 2007), solar and QBO signals (Matthes et al., 2013), as well as volcanic and solar signals (Chiodo et al., 2014). Usually this kind of interaction occurs at a specific location and time, which needs to be investigated in separate studies. Sophisticated attribution methods which can account for non-linearity have been used, such as machine learning methods (Blume et al, 2012), or optimal detection (Stott et al, 2003; Mitchell, 2016). Although these methods allow advanced statistics to be established, their limited interpretive capacities make it difficult to study physical mechanisms.

3 Solar signal

3.1 Surface temperature signal

As mentioned in the introduction, Zhou and Tung (2010; hereafter ZT2010) calculated CMDs between high- and low-activity periods of the 11-year solar cycle using the ERSST dataset. In their analysis, data near the World War II period (1942−1950) were excluded. We performed the same CMD analysis using the same dataset as ZT2010, but included all data from 1854 to 2007. We confirm the results of ZT2010 in Fig. 1a. The correlation coefficient between the expansion coefficients of the extracted pattern and the solar index shows a similar high correlation (0.69).

To assess the stability of the relationship between SSTs and the solar cycle, the use of a long dataset is crucial. However, historical datasets have problems with spatial coverage and inhomogeneity of the observing systems. This drawback may be compensated by a comparison with a recent global dataset assimilating satellite observations. Figure 1b shows the surface solar signal extracted by MLR using the ERA-I and F10.7 cm radio flux time series (solar index) as one of the explanatory variables for the period from 1979 to 2010. Despite the short time period of only 3 solar cycles, the results show a similar pattern in surface temperature to those obtained from longer historical datasets.

Common features in the spatial structure of the solar signal in surface temperatures include i) (sub-polar regions): warming around 45°−60°N over the Eurasian continent and cooling west of Greenland; ii) (mid-latitudes): warming over the ocean basins around 30°−45° latitudes in the Northern Hemisphere (NH) as well as in the Southern Hemisphere (SH); iii) (tropics): warming over the Indian Ocean and the central Pacific, and cooling in the East Pacific and the Atlantic, particularly in the SH. These characteristics are also found in a number of other studies cited in the introduction that use different analysis techniques.

To investigate the solar signals over the ocean basins specifically, equatorward gradients of climatological SSTs are shown in Fig. 1c. The regions where warming during solar maxima occurs roughly correspond to regions of strong meridional SST temperature gradients. The case of solar signals over the North Atlantic frontal zone is more complicated (see Fig. 1a), and in fact solar signals over the North Atlantic are delayed by 2–4 years (Gray et al., 2013; Scaife et al., 2013; Andrews et al. 2015; Thiéblemont et al., 2015), and will be discussed later. Note also that regions with cool solar signals in the tropics coincide with sectors of the cold tongue over the equatorial East Pacific and the Atlantic. This kind of temperature pattern is quite different from the expected impact of TSI variations from an energy balance model. Stevens and North (1996) estimated a warming in the tropics from such a model, in particular over the continents.

To identify the physical mechanisms responsible for the solar surface signals, a comparison of the surface temperature pattern associated with other forcings has been performed. The zonal-mean surface temperature pattern extracted by a MLR (see also Lean and Rind, 2008) is shown in Fig. 2 together with climatological zonal mean SSTs and their equatorward gradients. The latitudinal distribution of solar signals (Fig. 2a) is characterized by a mid-latitude warming and the absence of warming in the tropics. The El Niño–Southern Oscillation (ENSO) related temperature variations (Fig. 2d) are confined to the tropics. The response to volcanic aerosol (Fig. 2e) is a global cooling, whereas the response to anthropogenic greenhouse gas forcing (Fig. 2f) is characterized by a large warming in the polar region of the NH. A cooling trend is also found in the Southern Ocean around 60°S. However, it could also result from ozone depletion (Thompson et al., 2011), because trends in CO2 and ozone concentration cannot not be well separated due to the short analysis period. The fact that the amplitude of the solar signal is small in the tropics where ocean temperature (Fig. 2b) is high, but large in mid-latitude oceanic frontal regions (Fig. 2c), where the interaction between the atmosphere and the ocean is particularly strong (Nakamura et al., 2008), suggests a possible role of atmosphere–ocean interaction in the solar signal transfer.

The role of the Annular Mode (AM) (Thompson and Wallace, 2000) in the NH (NAM) in mediating tropospheric solar signals has been suggested by Baldwin and Dunkerton (2005). We examine the relationship between the solar signal and the NAM, as well as its counterpart in the Southern Hemisphere (SH), the SAM. The surface signal of NAM and SAM are also called Arctic Oscillation (AO) and Antarctic Oscillation (AAO), respectively. Figure 3 compares solar signals with annular modes in the two hemispheres. In NH winter (DJF), solar signals exhibit a similar pattern to the NAM: a warming over the Eurasian continent and the ocean basins along 30°N–45°N latitudes, and a cooling west of Greenland. Stronger westerly winds associated with the NAM and solar surface signals occur at lower latitudes over the American continent than over the Eurasian continent. This means that the NAM is not strictly annular, but also contains a stationary planetary wave structure. It should be noted that the spatial pattern of the solar signal is similar to that of the NAM.

In SH spring (SON), solar signals are characterized by a warming in mid-latitudes associated with anomalous westerlies around 40°S –50°S. However, the SAM pattern typically involves a strong warming around the Antarctic Peninsula and the

southern tip of the South American continent (Thompson and Wallace, 2000; Gillett et al., 2006) in association with anomalous westerlies near the polar region around 55°–65°S. Thus, in the SH, in contrast to the NH, solar signals are not related to the SAM (Lu et al., 2011).

3.2 Zonal-mean vertical structure

Since the solar surface signal during the recent (1979–2010) period is very similar to that of the longer historical period (1854–2007) (Fig. 1), we may gain further insight into the processes responsible for the solar signal transfer from the stratosphere to the troposphere and the ocean by analyzing the modern dataset in more detail. Figure 4 shows solar signals in the annual-mean a) zonal mean wind, b) zonal mean air temperature, and c) pressure coordinate vertical velocity in the tropical troposphere using the same MLR analysis as in Fig. 1b. The results of similar MLR analyses using meteorological reanalysis data have also been published (e.g., Frame and Gray, 2010; Chiodo et al., 2014; Mitchell et al., 2015a).

During periods of high solar activity, warming signals appear at three levels: the upper stratosphere–stratopause (5−1 hPa), the lower to middle stratosphere (100−20 hPa), and the troposphere (1000−300 hPa) (Fig. 4a). The warming around the stratopause extends globally from the tropics to the polar regions, while the warming in the lower stratosphere is confined to the tropics. The associated stronger meridional temperature gradient in the subtropical upper stratosphere is connected, by the thermal–wind relationship, to enhanced subtropical jets around 30°−40° latitude in both hemispheres in the upper stratosphere (Fig. 4b). Stronger subtropical jets extend farther to lower altitudes in association with a warming in the tropical lower stratosphere.

Previous studies suggest that the solar signal in the tropical lower stratospheric temperature is mainly induced through a modulation of the stratospheric mean meridional circulation or the Brewer-Dobson circulation (e.g. Kodera and Kuroda, 2002; Hood and Soukharev, 2012). Inspection of Figs. 5 and 6 reveals that the warming in the middle and lower stratosphere is produced in association with very sharp zonal wind anomalies. In fact, such strong meridional gradients of the zonal winds could not be produced by latitudinal difference of the radiative heating rate which mainly depends on the solar zenith angle. The differences in the latitudinal structure of the warming suggest that the warming in the stratopause–upper stratosphere has a radiative origin, while that in the middle to lower stratosphere has a dynamical origin.

In the troposphere, a statistically significant warming occurs in the extra-tropics around 40°−45° latitude in both hemispheres (Fig. 4a), similar to that of the surface temperature anomalies in Fig. 1. Warming also occurs over Antarctica in association with a weakening of the high-latitude westerly flow. Note that there is practically no warming in the entire tropical troposphere from the surface to the tropopause. This does not mean that there is no solar influence in this region, but temperature variations in the tropical troposphere are generally small due to feedback with convective activity (Eguchi et al., 2015). Therefore, the response in vertical velocity is crucial in the tropical troposphere, although it is not directly measured.

Solar signals in the vertical velocity in pressure coordinates are generally positive (downward) around the equator, but negative (upward) in off-equatorial regions around 15°−20° latitude (Fig. 4c).

Note also that solar signals in the zonal mean wind are symmetric around the equator in the upper stratosphere (Fig. 4b). However, in polar regions the zonal mean winds in the lower stratosphere differ markedly between the NH and SH. This can be seen more clearly as differences in the seasonal march in Fig. 5 for monthly solar signals in zonal mean winds during SH and NH winter. In early winter, the subtropical jet develops in the upper stratosphere in both hemispheres. In the NH, anomalous westerlies shift poleward and downward to the troposphere, and the stratospheric polar-night jet weakens significantly in February. In the SH, however, the poleward shift is small and the strong anomalous westerlies descend in the mid-latitude troposphere, forming a pair of westerly and easterly zonal mean wind anomalies at high latitudes in September.

Solar signals in zonal mean temperature and extracted by the MLR are shown in Fig. 6 (zonal mean zonal winds are also plotted in Fig. 6a with green lines). The lower stratospheric tropical warming occurs during a period when the stratospheric subtropical westerly winds develop, in July–August in the SH and in November–December in the NH. A tropospheric warming in mid-latitudes occurs in September−October in the SH and in January−February in the NH, and is associated with the downward penetration of westerly zonal mean wind anomalies from the stratosphere (Fig. 5). Thus, differences in the latitudinal structure of solar signals in Fig. 3 are explained by differences in the downward penetration in the two hemispheres. This downward penetration occurs through a modulation of the polar-night jet in the NH that projects onto the NAM, and a modulation of the subtropical jet in the SH which does not project onto the SAM.

3.3 Interactions with the ocean

The evolution from winter to spring of the solar signals in surface temperatures in the mid-latitudes of the NH is illustrated in Fig. 7a and 7b, respectively. In winter, stratospheric zonal mean wind anomalies extend from the stratosphere to the troposphere, and lead to a seesaw pattern between the polar region and mid-latitudes, similar to the NAM as shown in Fig. 3. In spring, stratospheric circulation anomalies vanish and therefore temperature anomalies over the continents weaken. However, temperature anomalies over the ocean basins east of the continents not only persist from winter but also continue to develop. The positive temperature anomalies over the North Pacific east of Japan extend along 40°N. In the Atlantic sector, positive temperature anomalies are located at lower latitudes along the southeastern US coastal region. A similar SST response in spring has been confirmed with a longer historical SST dataset from 1882 to 2008 (see Figure 4 of Tung and Zhou, 2010).

Note that temperature anomalies in the Pacific sector are created around ocean frontal zones, but in the Atlantic sector they are located at lower latitudes (Fig. 7c). However, the Atlantic anomalies shift northward along the Gulf Stream with time, as indicated by the lagged solar SST signals in Fig. 7d. When SST anomalies arrive around 45°N at 2 or 3 years after the solar

maximum, a meridional dipole pattern similar to the NAO develops (Gray et al., 2013; Scaife et al., 2013; Andrews et al., 2015; Thiéblemont, 2015) around the sub-Arctic frontal zone.

3.4. Tropical solar signals

Figure 8 shows the tropical part of the solar signal in SSTs extracted from the global picture in Fig. 1a. As mentioned previously, this pattern is characterized by a cooling over the East Pacific and the Atlantic in the SH and a warming in the central Pacific. To identify the characteristics of the spatial structure of these variations, an empirical orthogonal function (EOF) analysis is conducted on the SSTs over the tropical Pacific and the Atlantic sectors during September through February when ENSO shows the greatest persistence (Wolter and Timlin, 2011). The analysis period covers the years from 1890 to 2012. The leading and the second EOFs represent canonical ENSO and secular trends, respectively. The third EOF shows decadal variations and its spatial pattern is illustrated in Fig. 8b.

The solar signal (Fig. 8a) agrees well with the spatial structure of EOF3, which is characterized by a cooling over the cold tongue regions and a warming over the warm pool region in the central Pacific. This pattern of tropical SSTs, known as El Nino Modoki, has been extracted as EOF2 with a shorter dataset from 1979 through 2004 (Fig. 2b in Ashok et al., 2007). Unlike a canonical ENSO, there is a substantial meridional asymmetry in the SST field such that there is warming in the NH and cooling in the SH in EOF 3 as well as in the solar signal. Note that the solar signal has greater spatial extent, from the Pacific to Atlantic sectors, while that of EOF3 is confined mainly to the Pacific sector.

Cold tongues in tropical SSTs develop during boreal summer due to the Asian monsoon circulation (Wang, 1994). Therefore, the solar influence in the tropics is investigated for this season. Figure 9 shows correlation coefficients for boreal summer (JJA) between the solar index and a) SSTs, c) meridional wind velocity at 925 hPa, and e) out-going longwave radiation (OLR). Summertime climatologies are also displayed below the respective correlation plots; Figure 9b depicts climatological SSTs (contours) and their deviation from the zonal mean SST (color shading). The climatological northward component of the wind velocity at 925 hPa is displayed with 2 m s^{-1} contours (Fig. 9d). Figure 9e shows climatological OLR (color shading).

Regions of negative solar SST signals (Fig. 9a) roughly coincide with regions of low climatological SST with respect to the zonal mean, such as in the southeastern Pacific, the South Atlantic, and the coastal Arabian Sea. These sectors are also characterized by strong cross-equatorial winds along the continents (Fig. 9d). During periods of high solar activity a consistent increase in northward wind occurs in these regions (Fig. 9c). The correlation coefficients between the solar index (F10.7) and the OLR do not show a uniform increase of convective activity in the monsoon regions (lower OLR regions in Fig. 9f). The convective activity around the equatorial NH (0–10°N), such as over the Indian Ocean, South America, and Africa, is suppressed, while the convective activity of the off-equatorial NH (15°N–20°N) in the Asian sector tends to be

enhanced. Thus, the tropical solar influence is not characterized by a strengthening of the global monsoon circulation, but rather a northward shift of the convergence zone or the ascending branch of the Hadley circulation. This shift also introduces longitudinal structure in the SSTs due to the asymmetric distribution of the continents.

4 Stratosphere–troposphere dynamical coupling processes

The results of the observational analysis so far suggest that the solar surface signals in both the tropics and the extra-tropics originate from the stratosphere through changes in the stratospheric westerly jet. Because of strong and complex feedbacks inherent in the atmosphere–ocean system, it is not easy to understand from observations alone how stratospheric circulation changes globally affect the troposphere.

Therefore, we now compare the observed solar surface signals with the response obtained from a coupled atmosphere–ocean model experiment. In this experiment (Yukimoto and Kodera, 2007), stratospheric zonal winds are forced by the addition of zonal angular momentum in the winter stratosphere at levels above 100 hPa in the Meteorological Research Institute (MRI) coupled atmosphere–ocean general circulation model (MRI-CGCM2.3) (Yukimoto et al., 2006). The momentum forcing is essentially the same as that used by Thuburn and Craig (2000) except that the forcing (max: ±5 m s^{-1}/day) is applied only in the winter hemisphere with seasonal variations. See Yukimoto and Kodera (2007) for a more detailed description of the experiments.

Figure 10 shows the differences between the eastward and westward momentum (or strong and weak stratospheric westerly jet) experiments. Left- and right-hand panels are for July and January means of the last 50 years of a 100-year integration. The momentum forcing and zonal mean wind responses are shown in Fig. 10a and 10b. Although the momentum forcings are centered on 45° latitude in both hemispheres, the response in zonal mean winds differs in austral and boreal winters. A strengthening of the polar-night jet occurs in January, approximately poleward of 30°N in the NH, and zonal mean winds in the NH tropics decrease (noted by 'E' at the top of Fig. 10b). The deceleration occurs despite additional acceleration from the momentum forcing, due to the interaction with planetary waves. In contrast, in the SH in July, westerly winds weaken in the polar region.

Because stronger stratospheric westerly winds extend farther to lower latitudes in austral winter, a suppression of the ascending motion occurs more strongly in July in the tropics. As a consequence, stronger warming occurs around the tropical tropopause regions in July (Fig. 10d). Previous model studies (Thuburn and Craig, 2000; Kodera et al., 2011) showed that changes in stratospheric meridional circulation affect tropical convective activity through changes in static stability in the tropical tropopause region (Eguchi et al., 2015). In the present experiments also, suppression of equatorial ascending motion

occurs in the troposphere in connection with the reduction of stratospheric mean meridional circulation change, as can be seen in the residual circulation differences in Fig. 10c.

The extension of extra-tropical zonal mean wind anomalies from the stratosphere to the troposphere occurs in association with a change in tropospheric wave activity as indicated by the Eliassen–Palm (E–P) flux (Fig. 10e). Upward-propagating waves are deflected equatorward around the tropopause region (300 hPa) and produce easterly zonal mean wind anomalies in the subtropics, forming a pair of easterly and westerly zonal mean wind anomalies at higher latitudes. This anomalous zonal mean wind pattern also creates anomalous tropospheric warming around 40°N–45°N through the thermal wind balance. A particularly interesting response is found in the summer troposphere. Although no external forcing is applied in the summer hemisphere, an anomalous mid-latitude warming and wave activity persist in the troposphere, in particular in the SH. In fact, this latitudinal zone corresponds to the ocean frontal zone.

Figure 11a shows the horizontal structure of the annual mean SST differences between the stronger and weaker stratospheric westerly jet experiments, as in Fig. 10. This figure can be compared with the differences between high and low solar activity. The color shading in Fig. 11a shows the difference normalized by the standard deviation. Anomalous SST warming occurs around 40° latitude in both hemispheres, similar to the mid-latitude warming from the observations in response to the solar cycle in Fig. 1b. Cooling is also found in the equatorial southeastern Pacific and the Atlantic along the west coast of Africa, although it is quite small in the latter region. Note that the small response in the tropical Atlantic may be attributed to model deficiencies in low-level cloud formation. The cooling can be attributed to an increase of the cross-equatorial flow due to a suppression of rainfall near the equator, but an increase in off-equatorial regions (Fig. 11b). Cooling also appears in the coastal Arabian Sea in July (Fig. 11c) in connection with a strong northward meridional wind induced by an intensified Indian continent monsoon (Kodera, 2004). The increased convergence around the Indian continent is consistent with warming in the Bay of Bengal. These characteristics of the surface response to stratospheric westerly zonal wind changes fit well to the global solar surface signals from observations (Figs. 1 and 9).

5 Centennial scale variation

It is generally believed that changes in the solar UV produce regional effects in the troposphere, but have little impact on global mean temperatures (e.g., IPCC, 2013). However, this is not completely true for centennial solar variations. The effect of long-lasting weaker stratospheric polar vortices on tropospheric climate can be seen in the numerical experiment presented above. Figure 12 shows annual mean surface air temperature differences between weak and strong stratospheric westerly polar-night jet experiments averaged over the last 50 years, as in Fig. 11. The Earth's surface cools down remarkably. Global mean temperature decreases by about 0.5 K, although total solar irradiances are unchanged. This result arises because a weakening of the stratospheric polar vortex induces more frequent cold surges, which result in a larger snow

cover extent in mid-latitudes. As a consequence, the Earth's albedo increases and the radiative balance changes without change in the TSI. The spatial structure of the temperature anomaly thus obtained is quite similar to that estimated from proxy data (see Fig. 3 in Shindell et al., 2001): a cooling over eastern Canada, eastern Europe to Russia, and northeast Asia, as well as a warming over the west coast of North America, west of Greenland, and Kamchatka, although the warming of the Middle East is shifted a little southwestward. This very good agreement of the global spatial structure of the surface temperature changes suggests a dynamical origin of the cooling during the late Maunder Minimum period. This is consistent with the conclusion of Mann et al. (2009), that the temperature variations of the Little Ice Age and the Medieval Climate Anomaly are of dynamical origin. Thus, centennial-scale solar signals could also be explained by a change in the spectral distribution of solar irradiance, with changes only in the UV part of the solar spectrum, even if the change in total energy was negligibly small.

6 Discussion and concluding remarks

Through a comparison of different observation-based analyses of the solar influence on Earth's surface temperatures using historical and modern datasets, we have identified the following key features of the surface signal during a high solar activity:

1. Mid-latitude warming around the ocean frontal zones
2. No warming on average in the tropics with cooling in the cold tongue regions
3. Warming over the sub-polar Eurasian continent and cooling in the west of Greenland

Warming is also found over Antarctica with reanalysis data, which needs to be verified with more direct observational data.

Solar signals over the North Atlantic sector are small in Fig. 1, but the solar influence becomes apparent with a time delay of 2–3 years (Gray et al., 2013; Andrews et al. 2015, Thiéblemont et al., 2015). Scaife et al. (2013) demonstrated the role of ocean heat content producing a delayed effect. However, the calculated delays from a mechanistic model are too small to explain the observations. It is also important to explain why the solar response apparently lags only in the North Atlantic, but not in the North Pacific. Figure 3 showed that the solar signal has a similar structure to the AO in boreal winter. Warming signals in spring appear near the ocean frontal zone around 35° latitude in the Pacific (Fig. 7). Numerical experiments have suggested the important role of oceanic frontal zones in creating variability in the tropospheric zonal winds through modifications of baroclinic waves (Nakamura et al., 2008). Thus, in the Pacific, solar signals in the ocean frontal zone persist and induce large atmospheric impacts (Frankignoul and Sennéchael, 2007). Note that the spatial structures of the AO and NAO are not exactly the same, in particular over the east coast of the North American continent (Kodera and Kuroda, 2004; Wang et al., 2005). Compared with the Pacific sector, the warming in the Atlantic sector occurs at lower latitudes around 30°N, much farther south than the region of the ocean frontal zone in the North Atlantic (Fig. 7b). This means that the

original solar signal in the Atlantic sector is not well positioned to produce large atmospheric effects. The signal therefore needs 2–3 years before the SST anomalies are advected to the sub-polar frontal zone, where large amplification occurs by enhancing a NAO-like pattern (Fig. 7d).

Lower stratospheric tropical heating was proposed as possible origin of the solar influence on the troposphere (Haigh et al., 2005; Simpson et al., 2009). However, the reason for the warming in the tropical lower stratosphere during high solar activity is unclear. It has been shown that such tropical lower stratospheric warming is associated with a downward penetration of westerly anomalies from the upper stratosphere and hence of dynamical origin (Kodera and Kuroda, 2002). The mid-latitude warming on the Earth's surface through the solar signal is produced in association with the downward penetration of zonal mean wind anomalies from the upper stratosphere during winter to spring in both hemispheres (Fig. 5). A notable difference between the two hemispheres is that the tropospheric solar signal is more closely related to the polar-night jet variability in the NH, and to the upper stratospheric subtropical jet in the SH. These hemispheric differences can be attributed to different climatological seasonal marches in the stratospheric circulation due to differences in planetary wave activity (Kodera and Kuroda, 2002).

It should be noted that there are two kinds of westerly jets in the middle atmosphere. Figure 13 displays the climatological poleward temperature gradient during winter solstice (Jun in the SH and December in the NH). The meridional temperature gradient is large in the subtropics of the upper stratosphere due to solar UV heating, while in the lower stratosphere, the gradient is large in the polar region due to strong longwave cooling. They are respectively connected to the subtropical and polar night jet. Poleward and downward penetration of solar signals in the middle atmosphere occurs through interaction between these jets and planetary waves propagating from the troposphere.

To emphasize the initial role of the solar UV heating in the upper stratosphere, only the early winter situation was shown in Figure 15 of Kodera and Kuroda (2002). However, the stratospheric circulation evolves seasonally from a radiatively controlled to a dynamically controlled state. Here, we show these two stages schematically in Fig. 14 based on previous studies (Kodera and Kuroda, 2002; Matthes et al., 2006; Matthes et al., 2013). Increased solar UV heating in the tropics produces only a small increase in the subtropical jet in the case of no interaction with waves (Fig. 14a). However, such a small initial effect can be amplified through wave–mean flow interactions. During early winter, when planetary wave forcing is small, the waves (green arrows) are deflected at the stratopause subtropical jet (Fig. 14b). In this case, the downward extension of the subtropical jet occurs in association with significant tropical warming and mid-latitude cooling (Fig. 14b) as shown in Kodera and Kuroda (2002). In contrast, when planetary wave forcing becomes large enough in late winter to spring, the waves penetrate the subtropical upper stratosphere–stratopause region leading to a poleward shift of the westerly jet (Dunkerton, 2000) (Fig. 14c). Enhanced vertical wave propagation along the polar-night jet results in an increased convergence of waves in the upper stratosphere, on the one hand, while on the other hand it induces divergence in the lower

stratosphere, by which westerly anomalies descend into the polar region (Kuroda and Kodera, 1999). This results in a warming in the polar region of the upper stratosphere, but a cooling (or a reduction of the warming) in the tropical stratosphere due to an enhanced mean meridional circulation, as schematically illustrated in Fig. 14c.

Thus, the differences in the solar signal characteristics between the SH and the NH can be understood by the different durations of the radiatively and dynamically controlled stages related to different planetary wave activity. The solar signal in the NH is transmitted from the stratosphere to the surface through a poleward–downward shift of anomalous zonal mean wind, which creates a NAM-like structure in the troposphere. In the SH the planetary wave forcing is smaller, meaning the radiatively controlled stage lasts longer. As a consequence, the stratopause subtropical jet develops and extends to lower levels without a large poleward shift, meaning in turn that tropospheric solar signals in the SH do not resemble the SAM, which is related to variability in the polar-night jet.

To understand the solar signal, the overall features are investigated by combining the tropospheric part of Figs. 4, 5 and 6 in Fig. 15. The solar signal in the tropospheric temperature field is relatively small in January in the NH and September in the SH (Fig. 6; Fig. 15b). It should be noted that this is a period of transition; the tropospheric temperature signal is induced by the downward penetration of zonal wind anomalies. Therefore, more statistically significance should be expected in the zonal wind field (Fig. 5; Fig. 15a). A pair of warming and cooling is formed at both sides of the axis of the zonal mean zonal wind anomaly consistent with the thermal wind relationship. Therefore, the temperature signal is physically consistent even though the statistical significance is low. It is also shown in Fig. 7 that the surface temperature signal induced during the winter can be maintained and even amplified through an interaction with the ocean. Therefore a stronger statistically significant signal is found in the annual mean temperature field. In contrast, the annual mean zonal wind signal is less significant (Fig. 4). A possible role of ocean feedback to enhance stratospheric impact is also discussed in Yukimoto and Kodera (2007) and Misios and Schmidt (2013). The active role of the ocean is also found in the model experiment in Fig. 10 that although no external forcing is applied in the summer hemisphere, anomalous mid-latitude warming and wave activity persist in the troposphere, in particular in the SH.

This dynamical solar influence from the stratosphere can be reproduced by forcing stratospheric zonal mean winds in a coupled atmosphere–ocean general circulation model as shown in Figs. 10 and 11. A realistic numerical experiment with solar UV forcing in a general circulation model without an interactive ocean successfully reproduced the downward propagation of solar signals during NH winter (e.g., Matthes et al., 2006). More recent advanced middle atmosphere climate models, capable of reproducing upper stratospheric ozone variability as well as including the feedback to the ocean, can now simulate zonal mean wind variations with the solar cycle and their extension to the troposphere in both hemispheres as well as the observed differences in the NH and the SH (see e.g. Figs. 10 and 11 of Hood et al., 2015).

Van Loon et al. (2007) and Meehl et al. (2008, 2009) suggested that the tropospheric solar influence originates from an amplification by atmosphere–ocean interaction in the tropical Pacific; i.e., a modulation of the ENSO cycle. In particular, a La Niña-like SST anomaly, with cooling along the central to eastern equatorial Pacific, appears during solar peak (maximum) years. Roy and Haigh (2012) found a tendency for La Niña to occur more frequently during the peak year of the solar cycle. However, the peak year is only one of the 11 years of a full solar cycle. It seems more reasonable to consider that the ENSO cycle is modulated by the solar cycle, similarly to other internal modes of variability such as the AO, rather than suspecting that the tropospheric solar influence originates from a La Niña-like condition during the peak year of the solar cycle. The SST pattern related to the entire solar cycle extracted by ZT2010 with a CMD method shows a cooling in the tropical eastern Pacific. This spatial structure is different from the canonical ENSO pattern extracted as the leading EOF of tropical SSTs. The SST pattern associated with the solar cycle is similar to that of EOF3 in Fig. 8, which is characterized by a cooling in the cold tongue region in the southeastern Pacific, and a warming over the warm pool region in the central Pacific similar to the El Niño Modoki defined by Ashok et al. (2007). These authors also noted that the El Niño Modoki index exhibits a 12-year variation in addition to the 4-year interannual variation. This suggests a possible linkage to the solar cycle.

Cooling is also evident in the tropical South Atlantic Ocean in Fig. 8. The tropical Atlantic Ocean has no self-sustaining oscillation mode, unlike the tropical Pacific, but it can respond to external forcing with a north–south SST seesaw through the interaction of wind, evaporation, and SST (Xie and Tanimoto, 1998). Such a dipole pattern is discernible in Fig. 8. In fact, variations with the solar cycle of tropical Atlantic SSTs associated with cross-equatorial meridional winds have been reported (Lim et al., 2006; Suh and Lim, 2006). Thus, a concurrent cooling in the cold tongue regions suggests that the primary factor causing solar cycle variations in tropical SST is a northward shift of the convergence zone (i.e., the ascending branch of the Hadley cell) during boreal summer. Stronger southeasterly winds produce cooling in the equatorial SH west of the continents. These anomalies develop and are maintained through wind–evaporation–SST (WES) feedback, similar to that which creates a northward-displaced inter tropical convergence zone (ITCZ) in the climatological state (Xie, 2004). It is also evident that decreased cloud coverage due to fewer cosmic rays during high solar activity cannot explain such a cooling over the cold tongue regions, where low-level clouds usually form (Kristjánsson et al., 2004).

In summary, diverse aspects of the solar signal on the Earth's surface can be explained solely by solar UV heating changes in the upper stratosphere which penetrate to the troposphere through two pathways: the stratospheric westerly jet in the extra-tropics, and the stratospheric mean meridional circulation in the tropics, as suggested by Kodera and Kuroda (2002). It should also be noted that centennial circulation changes produced in the stratosphere can affect global mean surface temperature through changes in the Earth's surface condition without changes in total solar irradiance. The following processes, however, need further clarification: i) the role of ocean fronts and atmospheric baroclinic eddies in the downward

extension of zonal mean winds from the stratosphere, and ii) the role of tropical convection in interactions between the stratospheric mean meridional circulation and the Hadley circulation.

Acknowledgements

This work was supported in part by JSPS Grants-in-Aid for Scientific Research (S)24224011 and (C)25340010. KM and RT acknowledge support from the Helmholtz-University Young Investigators Group NATHAN funded by the Helmholtz-Association through the President's Initiative and Networking Fund and the GEOMAR Helmholtz Centre for Ocean Research Kiel. This work has been conducted within the frame of the WCRP/SPARC SOLARIS-HEPPA activity.

References

Andrews M.B., Knight J.R., Gray L.J: A simulated lagged response of the North Atlantic Oscillation to the solar cycle over the period 1960–2009. Environ. Res. Lett., 10, 054022. doi:10.1088/1748-9326/10/5/054022, 2015.

Austin, J., Tourpali, K., Rozanov, E. et al.: Coupled chemistry climate model simulations of the solar cycle in ozone and temperature, J. Geophys. Res., 113, D11306, doi:10.1029/2007JD009391, 2008.

Ashok K., Behera S.K., Rao S.A., Weng H., and Yamagata T.: El Niño Modoki and its possible teleconnection. J. Geophys. Res., 112, C11007, doi:10.1029/2006JC003798, 2007.

Baldwin M.P., and Dunkerton T.J.,: The solar cycle and stratosphere–troposphere dynamical coupling. J. Atmos. Sol.-Terr. Phys., 67, 71–82, 2005.

Blume, C., Matthes K., Horenko I.: Supervised learning approaches to classify sudden stratospheric warming events, J. Atmos. Sci., 69, 1824–1840, 2012.

Brohan P., Kennedy J.J., Harris I., Tett S.F.B., Jones P.D.: Uncertainty estimates in regional and global observed temperature changes: a new dataset from 1850. J. Geophys. Res., 111, D12106, doi:10.1029/2005JD006548, 2006.

Chiodo G, Marsh D, Garcia-Herrera R, Calvo N, Garca J. : On the detection of the solar signal in the tropical stratosphere. Atmos. Chem. Phys. 14 5251–5269, 2014.

Dee, D. P., Uppala, S. M., Simmons, A. J., et al.: The ERA-Interim reanalysis: configuration and performance of the data assimilation system, Q. J. Roy. Meteorol. Soc., 137, 553–597, 2011.

Dunkerton T.J.: Midwinter deceleration of the subtropical mesospheric jet and interannual variability of the high-latitude flow in UKMO analyses, J. Atmos. Sci., 57, 3838–3855, 2000.

Eguchi N., Kodera K., Nasuno T.: A global non-hydrostatic model study of a downward coupling through the tropical tropopause layer during a stratospheric sudden warming, Atmos. Chem. Phys., 15, 297–304, 2015

Frame T.H., Gray L.J.: The 11-year solar cycle in ERA-40 data: An update to 2008. J. Clim. 23 2213–2222, 2010.

Frankignoul C., Sennéchael N.: Observed influence of North Pacific SST anomalies on the atmospheric circulation. J. Clim., 20, 592–606, 2007.

Georgieva K., Kirov B., Tonev P., Guineva V., Atanasov D.: Long-term variations in the correlation between NAO and solar activity: The importance of north–south solar activity asymmetry for atmospheric circulation, Advances in Space Res., 40, 1152–1166, 2007.

Gillett N.P., Kell T.D., Jones P.D.: Regional climate impacts of the Southern Annular Mode, Geophys. Res. Lett., 33, L23704, doi:10.1029/2006GL027721, 2006.

Gray L. J., et al., Solar influence on climate, Rev. Geophys., 48, RG4001, doi:10.1029/2009RG000282., 2010.

Gray L.J., Scaife A.A., Mitchell D.M., Osprey S., Ineson S., Hardiman S., Butchart, N., Knight J., Sutton R., Kodera K., A lagged response to the 11 year solar cycle in observed winter Atlantic/European weather patterns, J. Geophys. Res., 118, 13,405–13,420, doi:10.1002/2013JD020062, 2013.

Haigh J.D., Blackburn M., Day R.: The response of tropospheric circulation to perturbations in lower-stratospheric temperature, J. Clim., 18, 3672–3685, doi:10.1175/JCLI3472.1. , 2005.

Hood, L. L., Soukharev, B. E.: The lower-stratospheric response to 11-yr solar forcing: Coupling to the troposphere–ocean response, J. Atmos. Sci., 69, 1841–1864, 2012.

Hood L. L., Misios S., Mitchell D.M., Rozanov E. et al.,: Solar signals in CMIP-5 simulations: The ozone response, Q. J. R. Meteorol. Soc., DOI 10.1002/qj.2553, 2015.

IPCC: Climate Change 2013, The physical science basis: Summary for policymakers, cambridge, UK, 2013.

Kaplan A, Cane M.A, Kushnir Y., Clement A.C., Blumenthal M.,B., Rajagopalan B.: Analyses of global sea surface temperature 1856–1991, J. Geophys. Res., 103, 18 567–18 589, 1998.

Kopp G., Lean J.L., A new, lower value of total solar irradiance: Evidence and climate significance, Geophys. Res. Lett., 38, L01706, doi:10.1029/2010GL045777, 2011.

Kodera K., Solar influence on the Indian Ocean monsoon through dynamical processes, Geophys. Res. Lett., 31, L24209, doi:10.1029/2004GL020928, 2004.

Kodera K., Kuroda Y.: Dynamical response to the solar cycle, J. Geophys. Res., 107(D24), 4749, doi:10.1029/2002JD002224, 2002.

Kodera, K., Kuroda Y.: Two teleconnection patterns involved in the North Atlantic/Arctic Oscillation, Geophys. Res. Lett., 31, L20201, doi:10.1029/ 2004GL020933, 2004.

Kodera K., Mukougawa H., Kuroda Y.: A general circulation model study of the impact of a stratospheric sudden warming event on tropical convection, SOLA, 7, 197−200, 2011.

Kuchar, A., Sacha, P., Miksovsky, J. and Pisoft, P. The 11-year solar cycle in current reanalyses: a (non)linear attribution study of the middle atmosphere. Atmos. Chem. Phys. 15, 6879–6895, 2015.

Kuroda Y. Kodera K., Role of planetary waves in the stratosphere-troposphere coupled variability in the northern hemisphere winter, Geophys. Res. Lett., 26, 2375-2378, 1999.

Kuroda, Y. Kodera K., Effect of the solar cycle on the Polar-night jet oscillation, J. Meteor. Soc. Jpn., 80, 973-984, 2002.

Kristjánsson J.E., Kristiansen, J., and Kaas, E.: Solar activity, cosmic rays, clouds and climate – an update, Adv. Space Res., 34, 407–415, 2004.

Lean J.L., Beer J, Bradley R.: Reconstruction of solar irradiance since 1610: implications for climate change, Geophys. Res. Lett., 23: 3195–3198, 1995.

Lean J.L., Rind D.H.: How natural and anthropogenic influences alter global and regional surface temperatures: 1889 to 2006, Geophys. Res. Lett., 35, L18701, doi:10.1029/2008GL034864, 2008.

Legras B., Mestre O., Bard E., Yiou P.: A critical look at solar-climate relationships from long temperature series. Clim. Past., 6, 745-758, 2010.

Lim G-H., Suh Y-C., Kim B-M.: On the origin of the tropical Atlantic decadal oscillation based on the analysis of the ICOADS, Q. J. R. Meteorol. Soc., 132, 1139–1152, 2006.

Lohmann G., Rimbu N., Dima M.: Climate signature of solar irradiance variations: Analysis of long-term instrumental, historical, and proxy data. Int. J. Climatol., 24, 1045–1056, doi: 10.1002/joc.1054, 2004.
2004.

Lu H., Gray L.J., Jarvis J., Baldwin M., High and low frequency 11-year solar cycle signature in the Southern Hemispheric winter and spring. Q. J. R. Meteorol. Soc. 137: 1641–1656, 2004, 2011.

Mann, M. E., et al.: Global signatures and dynamical origins of the Little Ice Age and Medieval Climate Anomaly, Science, 326, 1256–1260, doi:10.1126/science.1177303, 2009.

Marsh, D. R., Garcia R.R.: Attribution of decadal variability in lower stratospheric tropical ozone, Geophysical Research Letters, 34 (21), doi:10.1029/459 2007GL030935, 2007.

Matthes K., Kuroda Y., Kodera K., Langematz U.: Transfer of the solar signal from the stratosphere to the troposphere: Northern winter, J. Geophys. Res., 111, D06108, doi:10.1029/2005JD006283, 2006.

Matthes, K., Kodera, K., Garcia R.R., Kuroda Y., Marsh D.R., Labitzke K.: The importance of time-varying forcing for QBO modulation of the atmospheric 11 year solar cycle signal, J. Geophys. Res. Atmos., 118, 4435–4447, doi:10.1002/jgrd.50424, 2013.

Meehl G.A, Arblaster J. M., Branstator G., van Loon H.: A coupled air–sea response mechanism to solar forcing in the Pacific region. J. Climate, 21, 2883–2897, 2008.

Meehl G.A., Arblaster J.M., Matthes K., Sassi F., van Loon H.: Amplifying the Pacific climate system response to a small 11‐year solar cycle forcing, Science, 325, 1114–1118, doi:10.1126/science.117287, 2009.

Meinshausen M., Smith S.J., Calvin K.V., Daniel J.S., Kainuma M.L.T., Lamarque J.-F., Matsumoto K., Montzka S.A., Raper S.C. B., Riahi K., Thomson A.M., Velders G.J.M., van Vuuren D.: The RCP Greenhouse Gas Concentrations and their Extension from 1765 to 2300, Climatic Change 109, 213-241, DOI: 10.1007/s10584-011-0156-z., 2011.

Misios S, Schmidt H.: The role of the oceans in shaping the tropospheric response to the 11 year solar cycle. Geophys. Res. Lett. 40: 6373–6377, doi:10.1002/2013GL058439, 2013.

Mitchell D, Gray L, Fujiwara M, Hibino T, Anstey J, Ebisuzaki W, Harada Y, Long C, Misios S, Stott P, Tan D.: Signatures of naturally induced variability in the atmosphere using multiple reanalysis datasets. Q. J. R. Meteorol. Soc, 141, 2011–2031, doi: 10.1002/qj.2492, 2015a.

Mitchell, D., S. Misios, L.J. Gray, K. Tourpali, K. Matthes, L. Hood, H. Schmidt, G. Chiodo, R. Thiéblemont, E. Rozanov, D. Shindell, A. Krivolutsky: Solar signals in CMIP-5 simulations: The stratospheric pathway, Q. J. Roy. Met. Soc, doi:10.1002/qj.2530, 2015b.

Mitchell, D., Attributing the forced components of observed stratospheric temperature variability to external drivers, Q. J. Roy. Met. Soc, 142: 1041–1047, DOI:10.1002/qj.2707, 2016.

Nakamura H., Sampe T., Goto A., Ohfuchi W., Xie S.−P.: On the importance of midlatitude oceanic frontal zones for the mean state and dominant variability in the tropospheric circulation, Geophys. Res. Lett., 35, L15709, doi:10.1029/2008GL034010, 2008.

Nitta T., Yoshimura J.: Trends and interannual and interdecadal variations of global land surface air temperature. J. Meteor. Soc. Japan, 71, 367-375, 1993.

Pittock A.B.: A critical look at long-term sun-weather relationships, Rev. Geophys., 16, 400–420, 1978.

Rayner N.A., et al.: Global analyses of sea surface temperature, sea ice, and night marine air temperature since the late nineteenth century, J. Geophys. Res., 108(D14), 4407, doi:10.1029/2002JD002670, 2003.

Roy I, Haig J.D.: Solar cycle signals in the pacific and the issue of timings. J. Atmos. Sci., 69, 1446–1451. doi: http://dx.doi.org/10.1175/JAS-D-11-0277.1, 2012.

Sato M., Hansen J.E., McCormick M.P., Pollack J.B.: Stratospheric aerosol optical depth, 1850-1990. J. Geophys. Res., 98:22,987–22,994, 1993.

Scaife A.A., Ineson S., Knight J.R., Gray L.J., Kodera K., Smith D.M.:A mechanism for lagged North Atlantic climate response to solar variability, Geophys. Res. Letts., 40, 434–439, doi:10.1002/grl.50099, 2013.

Shindell D.T., Schmidt G.A., Miller R.L., Rind D.: Northern Hemisphere winter climate response to greenhouse gas, ozone, solar, and volcanic forcing. J. Geophys. Res., 106, 7193-7210, doi:10.1029/2000JD900547, 2001.

Smith T.M., Reynolds R.W, Peterson T.C., Lawrimore J.: Improvements NOAAs Historical Merged Land-Ocean Temp Analysis (1880-2006), J. Clim., 21, 2283-2296, 2008.

Souza-Echer M.P., Echer E, Rigozo N.R., Brum C.G.M., Nordemann, D.J.R., Gonzalez W.D.: On the relationship between global, hemispheric and latitudinal averaged air surface temperature (GISS time series) and solar activity, J. Atmos. Solar-Terr. Phys., 74, 87–93, 2012.

Stott, P.A., Jones G., Mitchell J.F.B.: Do models underestimate the solar contribution to recent climate change? J. Clim. 16: 4079–4093, 2003.

Suh Y.-C., Lim G.-H.: Effects of the 11-year solar cycle on the Earth atmosphere revealed in ECMWF reanalyses, Geophys. Res. Lett., 33, L24705, doi:10.1029/2006GL028128, 2006.

Simpson, I., Blackburn M, Haigh J. D.: The role of eddies in driving the tropospheric response to stratospheric heating perturbations, J. Atmos. Sci., 66, 1347–1365, 2009.

Stevens M.J., North G.R.: Detection of the climate response to the solar cycle. J. Atmos. Sci., 53, 2594–2608,1996.

Svensmark H., Friis-Christensen E.: Variation of cosmic ray flux and global cloud coverage - A missing link in solar-climate relationships, J. Atmos. Sol.. Terr. Phys,. 59, 225-1232,1997.

Tapping K. F.: The F10.7 cm solar radio flux ($F_{10.7}$), Space Weather, 11, 394-406, doi:10.1002/swe.20064, 2013.

Thiéblemont R., Matthes K., Omrani N-E, Kodera K., Hansen F.: Solar forcing synchronizes decadal North Atlantic climate variability, Nature Communications, doi: 10.1038/ncomms9268, 2015.

Thompson, D.W.J., Wallace J.M.: Annular modes in the extratropical circulation. Part I: Month-to-month variability. J. Climate, 13, 1000–1016, 2000.

Thompson, D.W.J., Solomon S., Kushner P.J., England M.H., Grise K.M., Karoly D.J.: Signatures of the Antarctic ozone hole in Southern Hemisphere surface climate change, Nat. Geosci., 4(11), 741–749, 2011.

Thuburn J., Craig G.C.: Stratospheric influence on tropopause height: The radiative constant. J. Atmos. Sci., 57, 17– 28, 2000.

Tiao G, Reinsel G., Xu D., Pedrick J., Zhu X., Miller A., DeLuisi J., Mateer C., Wuebbles D.: Effects of autocorrelation and temporal sampling schemes on estimates of trend and spatial correlation. J. Geophys. Res.: Atmos., 95: 20 507–20 517, doi: 10.1029/JD095iD12 p20507, 1990.

Tung K.K., Zhou J.S.: The Pacific's response to surface heating in 130 yr of SST: La Niña–like or El Niño–like? J. Atmos. Sci., 67, 2649–2657, 2010.

van Loon H., Meehl, G.A., Shea, D.J.: Coupled air-sea response to solar forcing in the Pacific region during northern winter, J. Geophys. Res., 112(D2), D02108, doi:10.1029/2006JD007378, 2007.

Wang Y.-M., Lean J., Sheeley N.R.Jr: Modeling the Sun's magnetic field and irradiance since 1713. Astrophys. J., 625, 522–538, 2005.

Wang B.: On the annual cycle in the tropical eastern central Pacific. J. Clim., 7, 1926–1942, 1994.

Wang D., Wang C., Yang X., Lu J.: Winter Northern Hemisphere surface air temperature variability associated with the Arctic Oscillation and North Atlantic Oscillation, Geophys. Res. Lett., 32, L16706, doi:10.1029/2005GL022952, 2005.

Wolter K., Timlin, M.S.: El Niño/Southern Oscillation behaviour since 1871 as diagnosed in an extended multivariate ENSO index (MEI.ext). Int. J. Climatol., 31: 1074–1087. doi: 10.1002/joc.2336, 2011.

Xie S.-P.: The shape of continents, air-sea interaction, and the rising branch of the Hadley circulation. In The Hadley Circulation: Past, Present and Future, H. F. Diaz and R. S. Bradley (eds.), Kluwer Academic Publishers, Dordrecht, 121-152, 2004.

Xie S.-P., Tanimoto Y.: A pan-Atlantic decadal climate oscillation, Geophys. Res. Lett., 25, 2185-2188, 1998.

Yukimoto S., Noda A., Uchiyama S., Kusunoki T., Kitoh A.: Climate change of the twentieth trough twenty-first centuries simulated by the MRI-CGCM2.3. Pap. Meteor. Geophys., 56, 9−24, 2006.

Yukimoto S., Kodera K.: Annular modes forced from the stratosphere and interactions with the ocean, J. Meteorol. Soc. Jpn., 85, 943–952, 2007.

Zhou J.S., Tung K.K.: Solar cycles in 150 years of global sea surface temperature data. J. Climate, 23, 3234–3248, 2010.

Figure captions

Figure 1: T a) Annual mean SST anomaly extracted by the same CMD analysis as in Zhou and Tung (2010) for the period 1854-2007. b) Annual solar index regression coefficient of the surface temperature derived by applying the MLR model to ERA-I data for the period 1979–2010. Stippled areas indicate statistical significance at the 95% level. c) Equatorward gradient of annual mean climatological SST.

Figure 2: MLR analysis of the annual zonal mean surface temperature from ERA-I, calculated for the period 1979–2010, for (a) solar activity, (d) ENSO, (e) volcanic activity, and (e) CO_2 concentration. Climatological zonal mean SSTs and their equatorward meridional gradient are also shown in (c) and (b), respectively.

Figure 3: Solar regression coefficient extracted by the MLR technique for the DJF mean NH (a) 500 hPa zonal mean wind, and (b) surface temperature. (c and d) Same as (a and b), but for the SON mean in the SH. (e and f) Same as (a and b), except for the correlation with surface NAM index. (g and h): same as (c and d), except for the surface SAM index. The period of analysis is 1979–2010. Stippled regions indicate statistical significance at the 90% level.

Figure 4: Solar regression coefficients of the annual-zonal mean a) air temperature, b) zonal wind, and c) vertical velocity in the tropical troposphere. Solid (dashed) contours indicate positive (negative) values and are drawn every (a) 0.25 K, (b) 0.5 m s^{-1}, and (c) 5 m /day. Areas of 90% and 95% statistical significance are shown by light and dark shading, respectively, in red (positive) and blue (negative).

Figure 5: Monthly solar regression coefficient of zonal-mean zonal winds in (left) July, August, September, and October in the SH, and (right) November, December, January, and February in the NH. Solid (dashed) contours indicate positive (negative) values and are drawn every 1 m s^{-1}. Areas of 90% and 95% statistical significance are shown by light and dark shading, respectively, in red (positive) and blue (negative).

Figure 6: (a) Same as Fig. 5, except for 2-month mean air temperature, July–August in the SH (left), and November–December in the NH (right). Green lines indicate 2 m s^{-1} contours of the corresponding zonal mean zonal wind. (b) Same as (a), except for monthly mean temperature in September (left) and January (right). (c) Same as (b), except for October (left) and February (right). Contour interval for temperature is 0.5K.

Figure 7: (a and b) Solar regression coefficient of the surface temperature (at 1000 hPa) over the NH mid-latitudes for (a) DJF and (b) MAM. c) Climatological mean SST in spring (MAM). d) Solar regression coefficients of SST in the North Atlantic sector extracted from ERSST (1880 to 2010) at lag times of 0, 1, 2, and 3 years. Horizontal lines indicate 45°N. Stippled areas indicate statistical significance at the 90% level.

Figure 8: (a) Same as Fig. 1a, except for the tropical Pacific and Atlantic sectors only (30°S−30°N, 120°E–20°E). (b) SST spatial structure of the third EOF in September–February for the period 1890–2012 (Color shading). Contours indicate climatological SST.

Figure 9: Boreal summer (JJA) solar signal in (a) SST, (c) meridional winds at 925 hPa, and (e) OLR, presented as correlations with the solar index for the period 1979–2010. b) JJA mean climatological SST, with contours for 27°, 28°, and 29°C, and color shading denoting the deviation from the latitudinal mean SST. d) Climatological JJA northward wind component at 925 hPa (contours every 2 m s^{-1}). f) Climatological JJA OLR (color shading).

Figure 10: Difference between strong and weak stratospheric westerly jet experiments by Yukimoto and Kodera (2007) in July (left) and January (right): (a) Zonal momentum forcing (m s^{-1}/day), (b) zonal-mean zonal winds (m s^{-1}), (c) mean meridional residual circulation (10^9 kg s^{-1}), (d) zonal-mean air temperature (K), and (e) E–P fluxes (m^2 s^{-2}) (arrows) and their divergence (color shading). Color shading indicates differences normalized by the standard deviation.

Figure 11: a) Differences in the annual mean SST between strong and weak stratospheric westerly jet experiments, similar to Fig. 10. b) Same as (a), except for the annual mean precipitation. c) Same as (a), except for July mean SST in the Indian Ocean sector. Units are (a) K, (b) mm/day, and (c) K. Color shading indicates regions where statistical significance exceeds the 95% level.

Figure 12: Similar to Fig. 11, except for annual mean surface temperature differences between weak and strong stratospheric westerly jet experiments, comparable to an extended period of extreme solar minimum (Maunder Minimum-like) conditions. Color shading indicates regions where statistical significance exceeds the 95% level.

Figure 13: Meridional sections of the climatological poleward temperature gradient around the winter solstice: (a) SH June, (b) NH December.

Figure 14: Schematic presentation of the solar influence on the winter stratosphere. (a) Hypothetical response to solar UV heating without interaction with planetary waves. (b) Early winter when solar radiative forcing dominates, and (c) late winter when dynamical forcing from the troposphere becomes more important. See text for details.

Figure 15: (a) Same monthly solar regression coefficient of zonal-mean zonal winds as in Fig. 5, except for the tropospheric part: (left) SH in September, and (right) NH in January. (b) Same as in (a), except for the temperature signal in Fig. 6. (c) Tropospheric part of solar regression coefficients of the annual-zonal mean air temperature in Fig. 4a. Contour intervals are 0.25K for temperature and 1 ms^{-1} for wind.

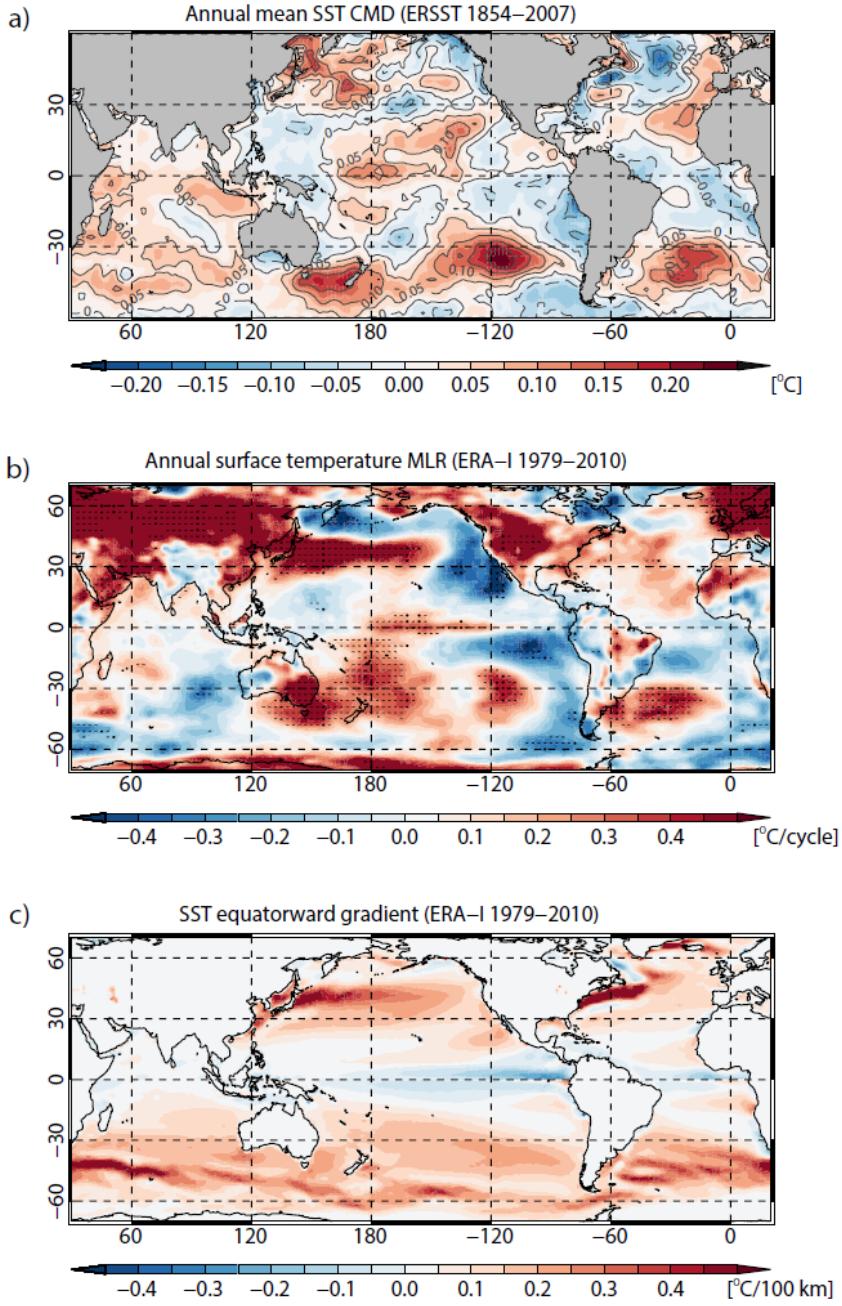
a)
Annual mean SST CMD (ERSST 1854–2007)
30
0
–30
60
120
180
–120
–60
0
–0.20 –0.15 –0.10 –0.05 0.00 0.05 0.10 0.15 0.20
[°C]
b)
Annual surface temperature MLR (ERA–I 1979–2010)
60
30
0
–30
–60
60
120
180
–120
–60
0
–0.4 –0.3 –0.2 –0.1 0.0 0.1 0.2 0.3 0.4
[°C/cycle]
c)
SST equatorward gradient (ERA–I 1979–2010)
60
30
0
–30
–60
60
120
180
–120
–60
0
–0.4 –0.3 –0.2 –0.1 0.0 0.1 0.2 0.3 0.4
[°C/100 km]

Fig. 1

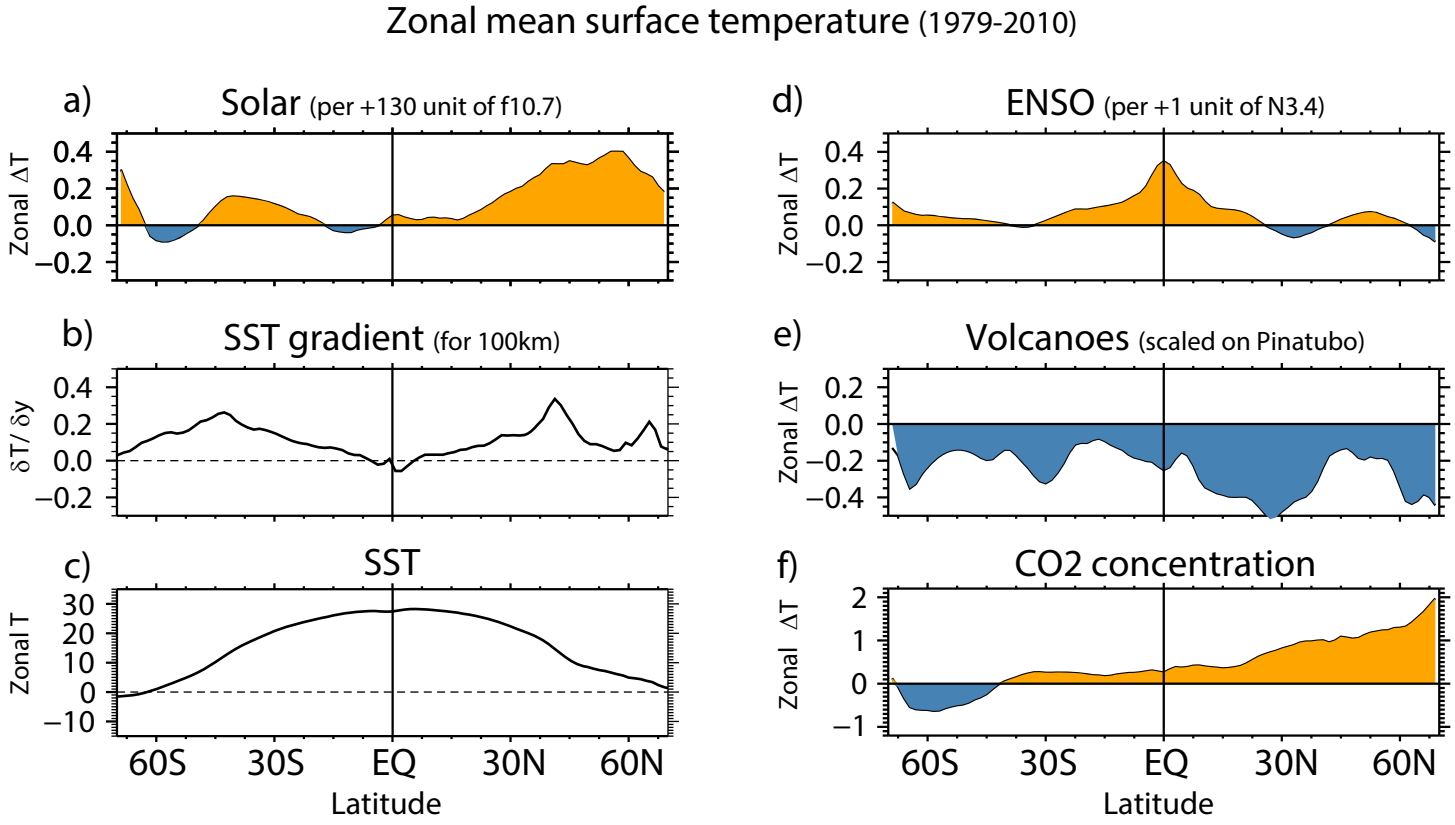
Zonal mean surface temperature (1979-2010)
a)
Solar (per +130 unit of f10.7)
Zonal ΔT
0.4
0.2
0.0
−0.2
b)
SST gradient (for 100km)
δT/ δy
0.4
0.2
0.0
−0.2
c)
SST
Zonal T
30
20
10
0
−10
60S
30S
EQ
30N
60N
Latitude
d)
ENSO (per +1 unit of N3.4)
Zonal ΔT
0.4
0.2
0.0
−0.2
e)
Volcanoes (scaled on Pinatubo)
Zonal ΔT
0.2
0.0
−0.2
−0.4
f)
CO2 concentration
Zonal ΔT
2
1
0
−1
60S
30S
EQ
30N
60N
Latitude

Fig. 2

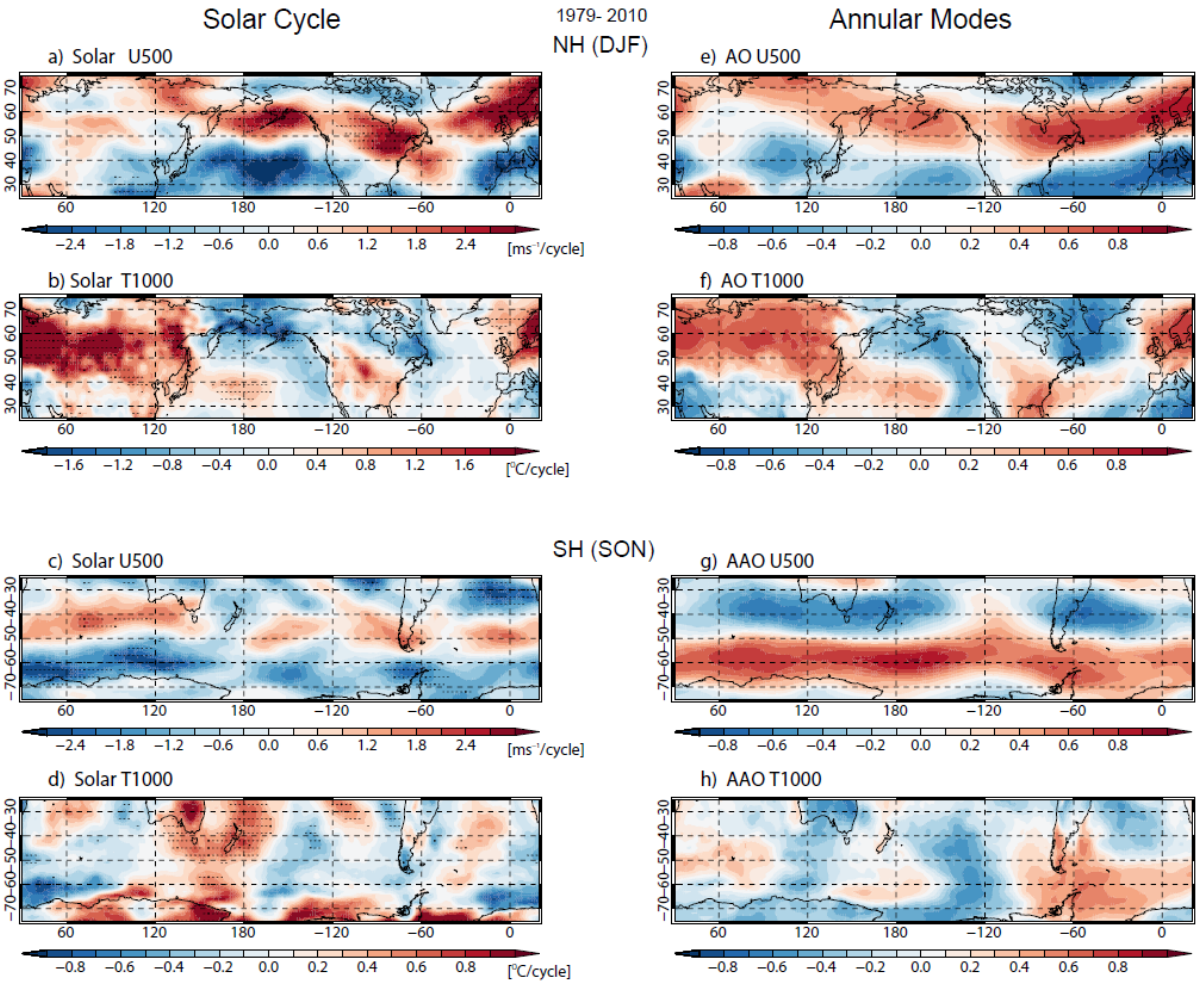
Solar Cycle
1979- 2010
Annular Modes
NH (DJF)
a) Solar U500
e) AO U500
b) Solar T1000
f) AO T1000
SH (SON)
c) Solar U500
g) AAO U500
d) Solar T1000
h) AAO T1000
[ms⁻¹/cycle]
[°C/cycle]

Fig. 3

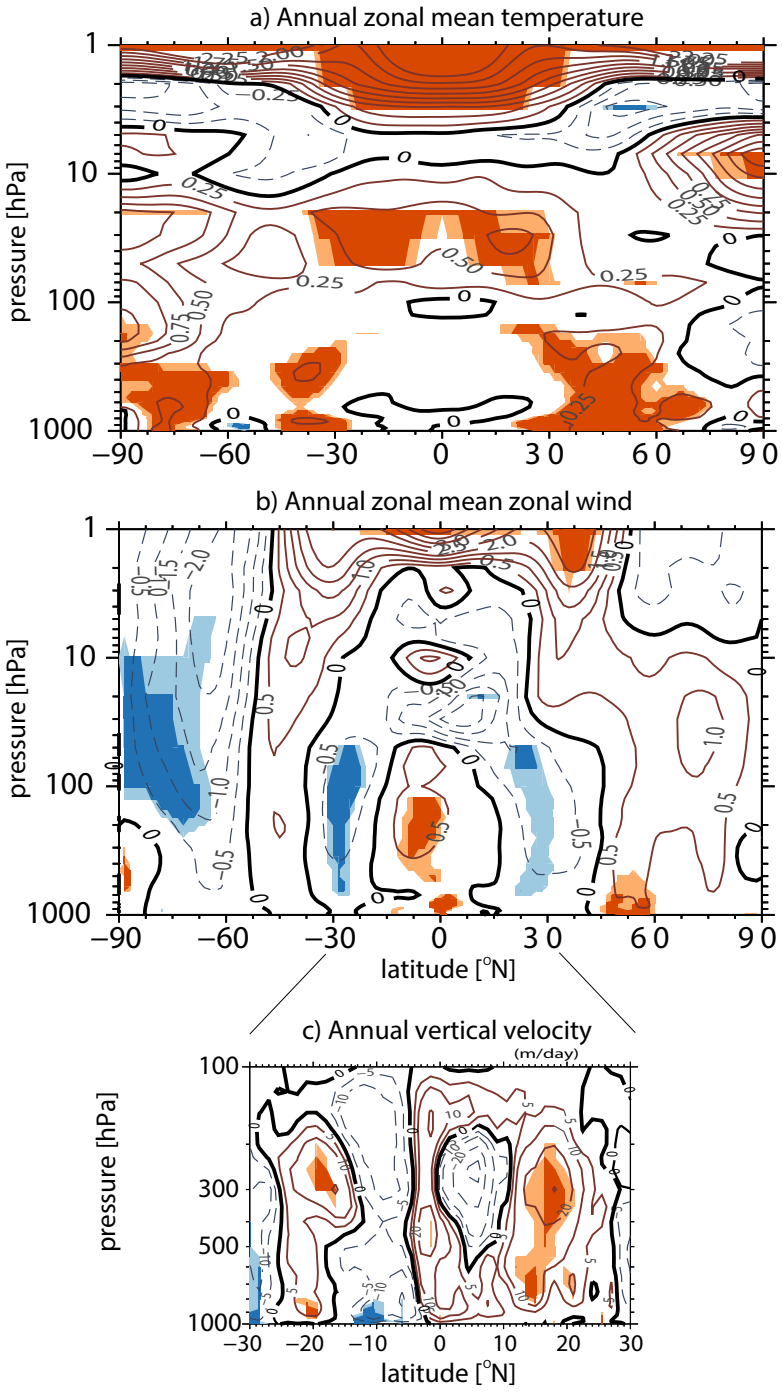
a) Annual zonal mean temperature
pressure [hPa]
1
10
100
1000
−90
−60
−30
0
30
60
90
b) Annual zonal mean zonal wind
pressure [hPa]
latitude [°N]
c) Annual vertical velocity
(m/day)
pressure [hPa]
100
300
500
1000
−30
−20
−10
0
10
20
30
latitude [°N]

Fig. 4

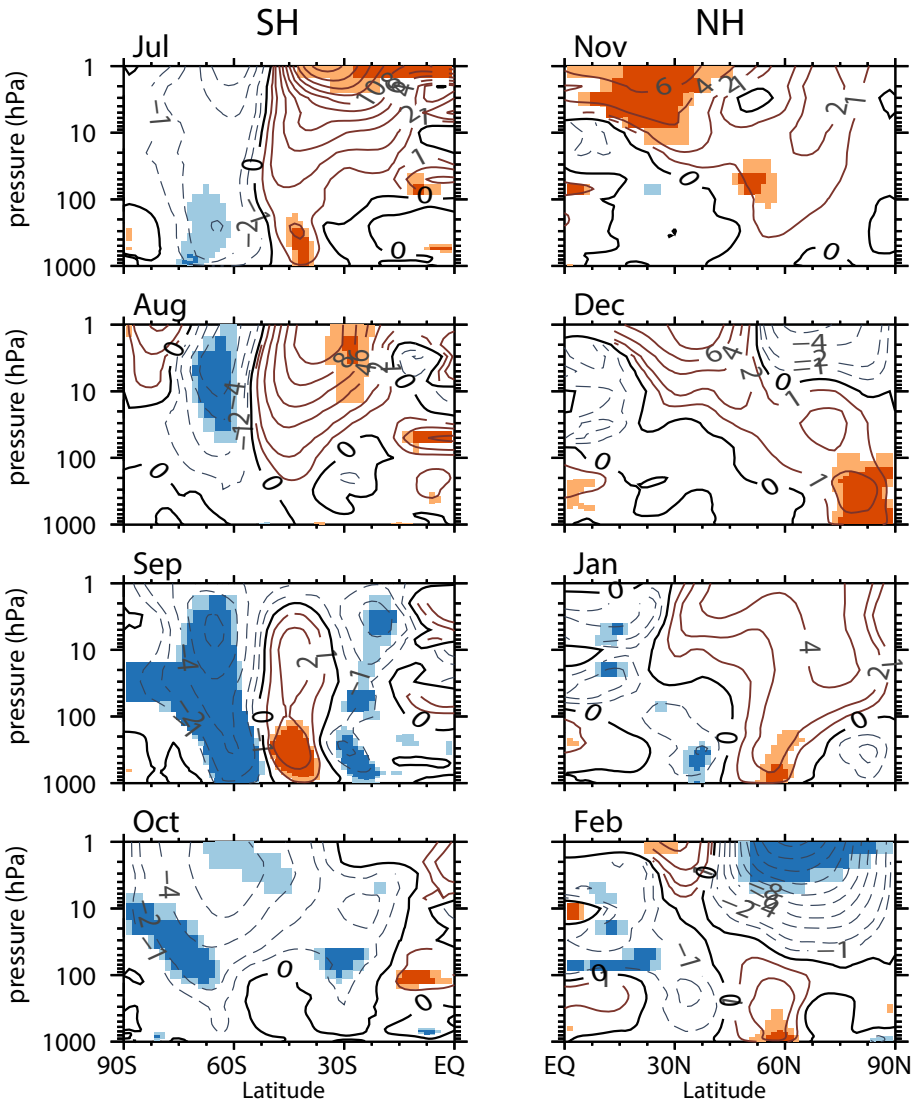
SH
NH
Jul
Nov
Aug
Dec
Sep
Jan
Oct
Feb
pressure (hPa)
1
10
100
1000
90S
60S
30S
EQ
EQ
30N
60N
90N
Latitude
Latitude

Fig. 5

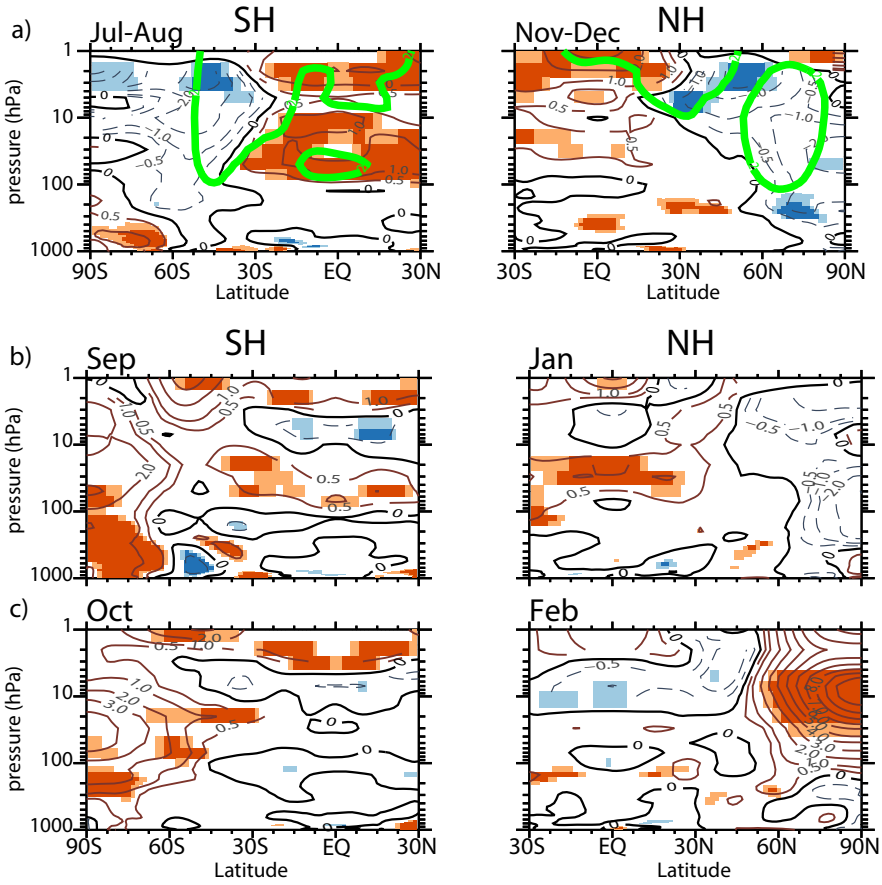
a)
Jul-Aug
SH
Nov-Dec
NH
b)
Sep
SH
Jan
NH
c)
Oct
Feb
pressure (hPa)
1
10
100
1000
90S
60S
30S
EQ
30N
60N
90N
Latitude

Fig. 6

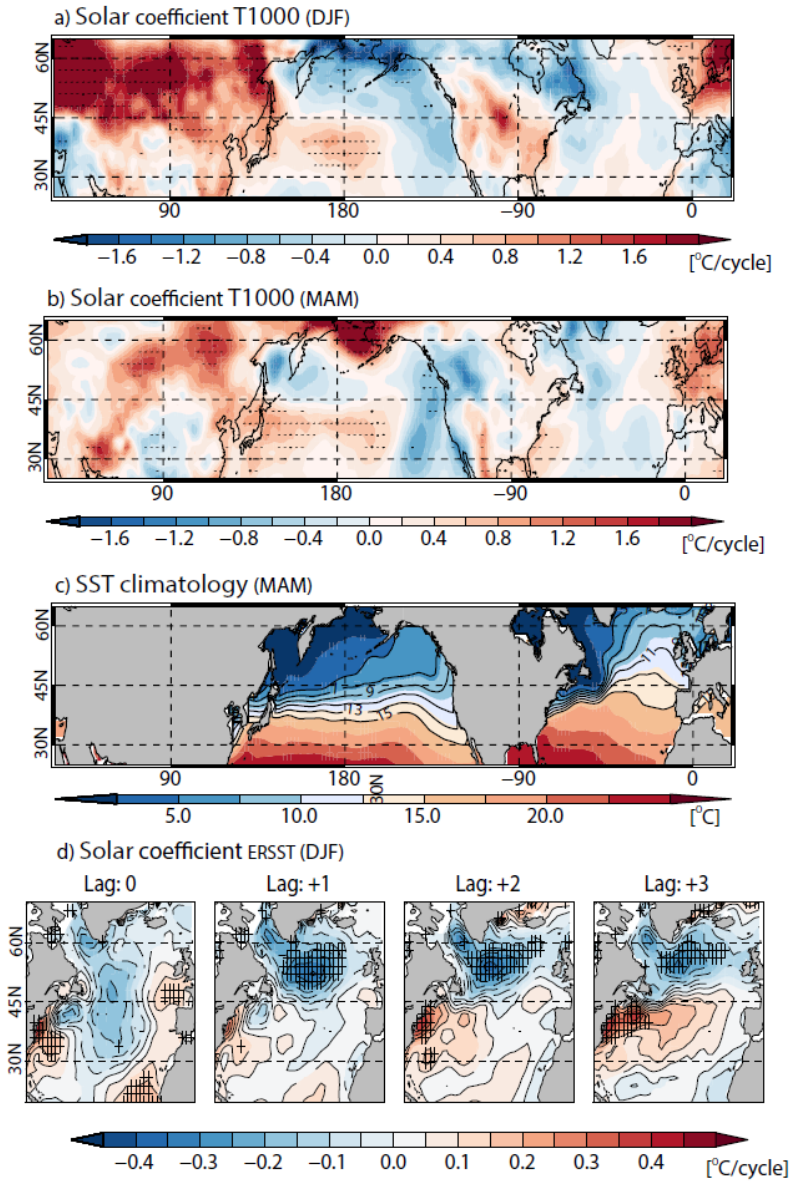
a) Solar coefficient T1000 (DJF)
60N
45N
30N
90
180
−90
0
−1.6 −1.2 −0.8 −0.4 0.0 0.4 0.8 1.2 1.6
[°C/cycle]
b) Solar coefficient T1000 (MAM)
60N
45N
30N
90
180
−90
0
−1.6 −1.2 −0.8 −0.4 0.0 0.4 0.8 1.2 1.6
[°C/cycle]
c) SST climatology (MAM)
60N
45N
30N
90
180
−90
0
5.0 10.0 15.0 20.0
[°C]
d) Solar coefficient ERSST (DJF)
Lag: 0
Lag: +1
Lag: +2
Lag: +3
60N
45N
30N
−0.4 −0.3 −0.2 −0.1 0.0 0.1 0.2 0.3 0.4
[°C/cycle]

Fig. 7

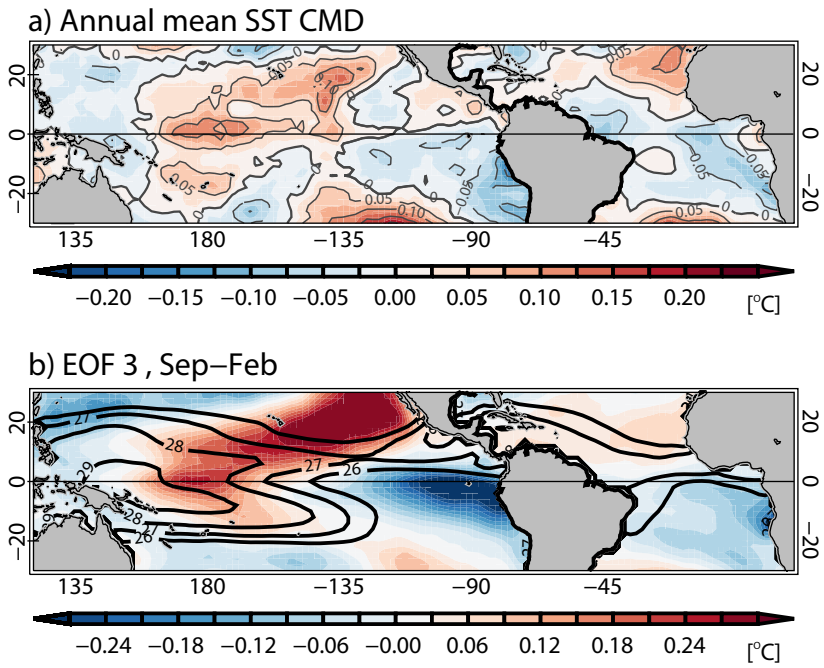
a) Annual mean SST CMD
20
0
−20
135
180
−135
−90
−45
−0.20 −0.15 −0.10 −0.05 0.00 0.05 0.10 0.15 0.20
[°C]
b) EOF 3 , Sep−Feb
20
0
−20
135
180
−135
−90
−45
−0.24 −0.18 −0.12 −0.06 −0.00 0.06 0.12 0.18 0.24
[°C]

Fig. 8

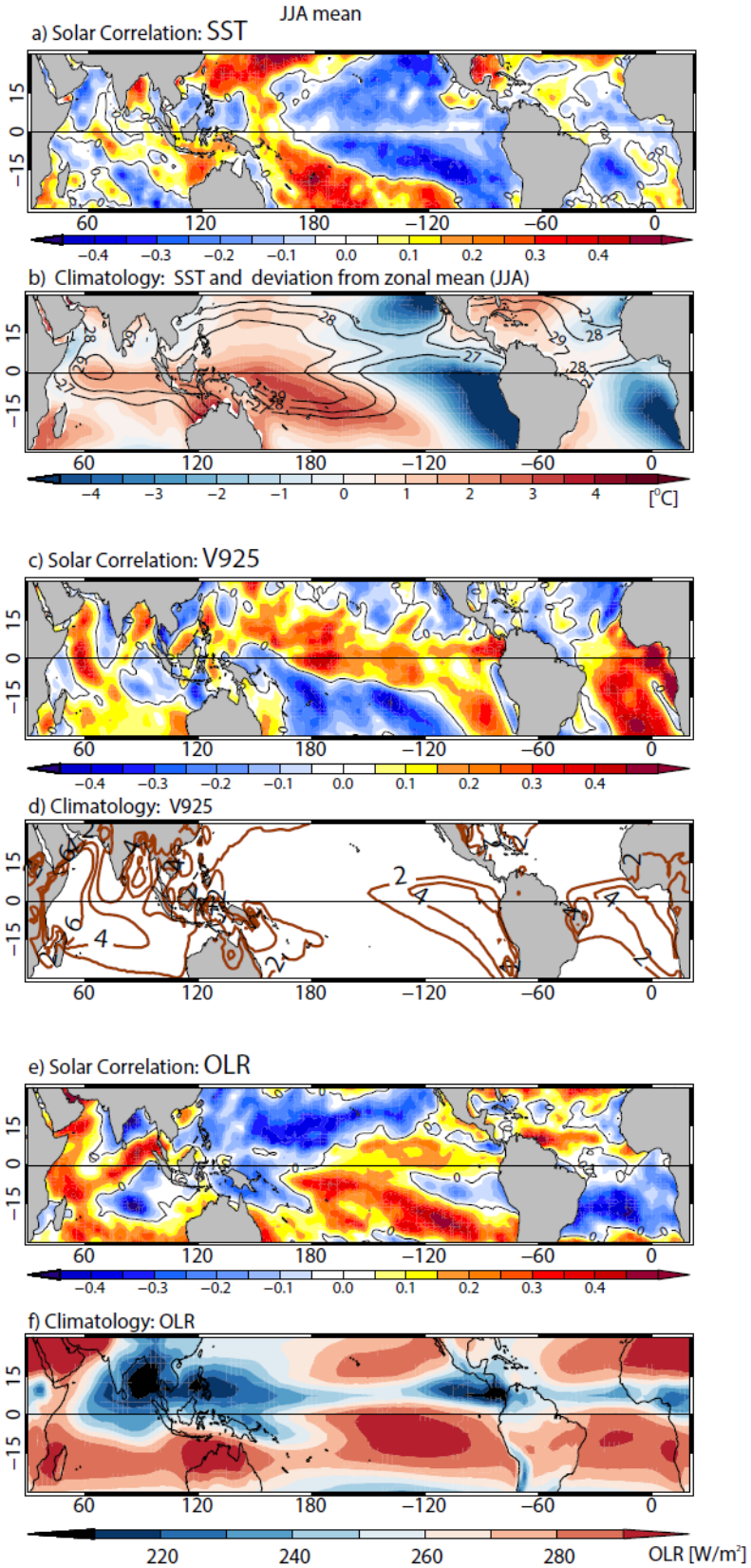
JJA mean
a) Solar Correlation: SST
b) Climatology: SST and deviation from zonal mean (JJA)
[°C]
c) Solar Correlation: V925
d) Climatology: V925
e) Solar Correlation: OLR
f) Climatology: OLR
OLR [W/m²]

Fig. 9

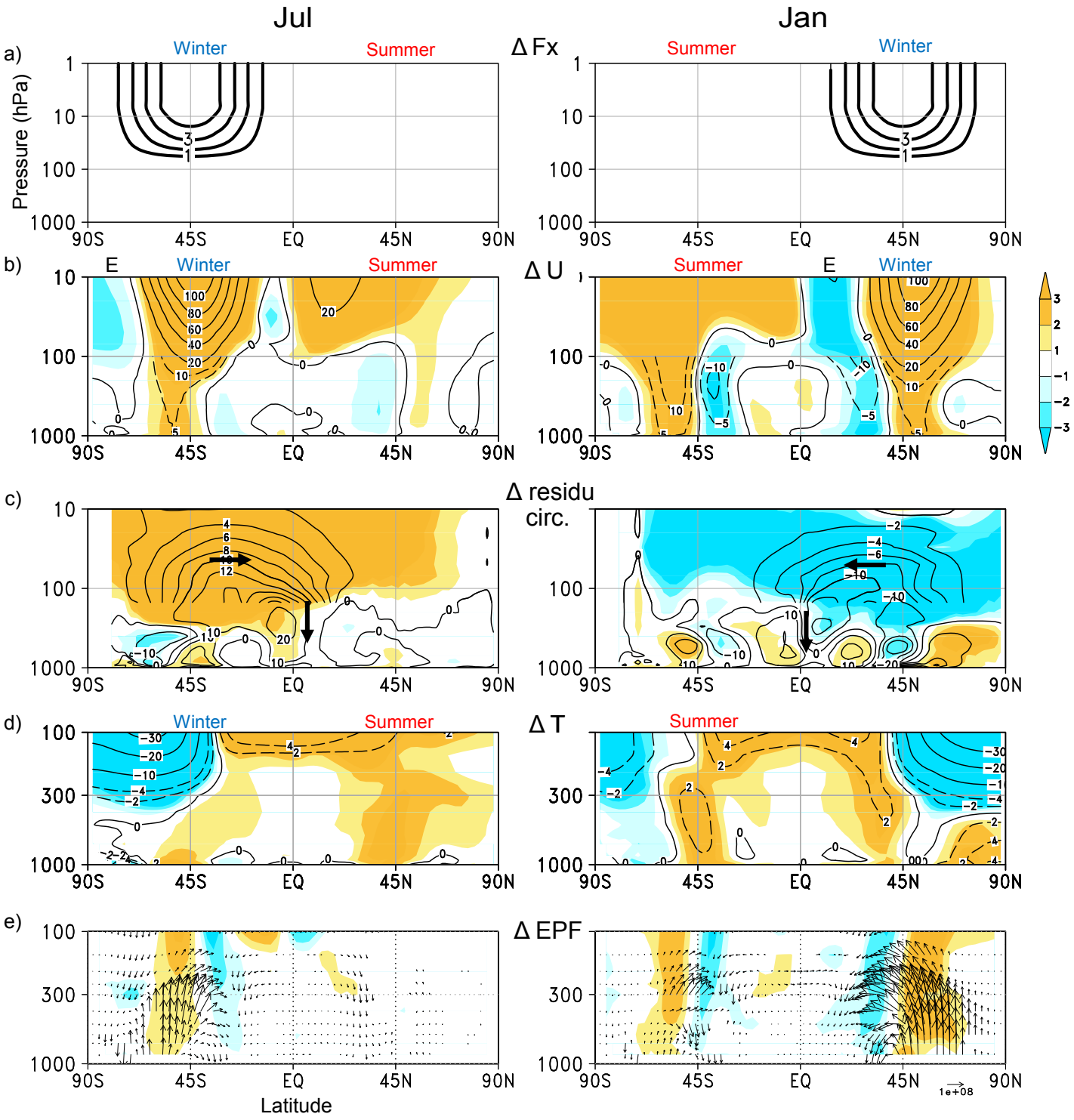
Jul
Jan
a)
Winter
Summer
Δ Fx
Pressure (hPa)
b)
E
Δ U
c)
Δ residu
circ.
d)
Δ T
e)
Δ EPF
90S
45S
EQ
45N
90N
Latitude
1e+08

Fig. 10

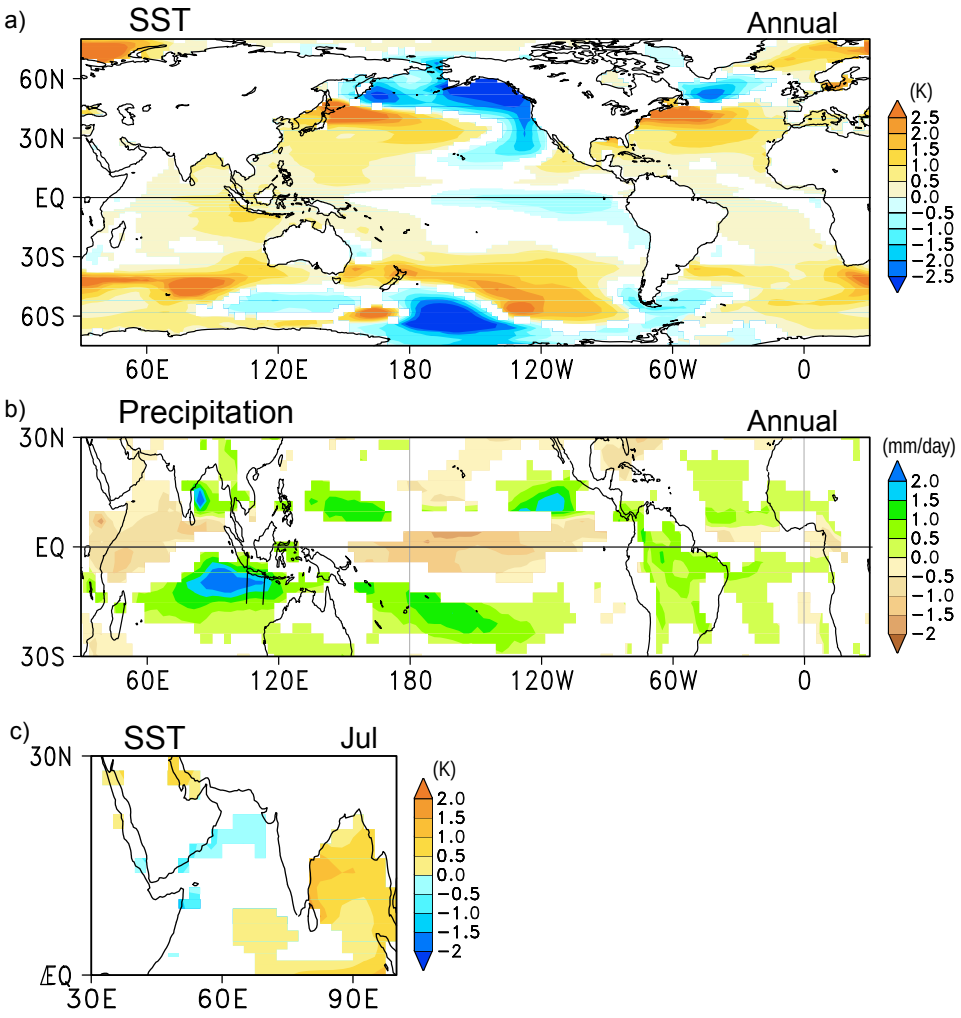
a)
SST
Annual
60N
30N
EQ
30S
60S
60E
120E
180
120W
60W
0
(K)
2.5
2.0
1.5
1.0
0.5
0.0
−0.5
−1.0
−1.5
−2.0
−2.5
b)
Precipitation
Annual
30N
EQ
30S
60E
120E
180
120W
60W
0
(mm/day)
2.0
1.5
1.0
0.5
0.0
−0.5
−1.0
−1.5
−2
c)
SST
Jul
30N
ÆQ
30E
60E
90E
(K)
2.0
1.5
1.0
0.5
0.0
−0.5
−1.0
−1.5
−2

Fig. 11

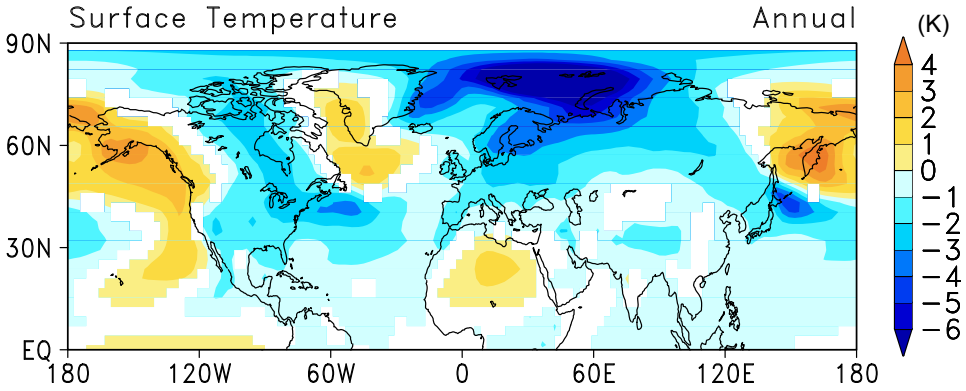
Surface Temperature
Annual
(K)
4
3
2
1
0
−1
−2
−3
−4
−5
−6
90N
60N
30N
EQ
180
120W
60W
0
60E
120E
180

Fig. 12

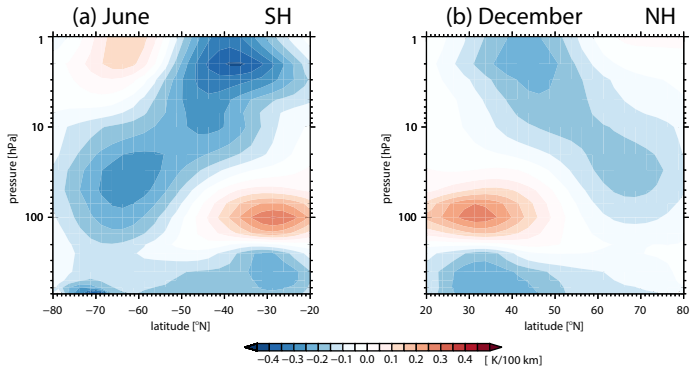
(a) June
SH
(b) December
NH
pressure [hPa]
1
10
100
−80
−70
−60
−50
−40
−30
−20
latitude [°N]
20
30
40
50
60
70
80
−0.4 −0.3 −0.2 −0.1 0.0 0.1 0.2 0.3 0.4 [K/100 km]

Fig. 13

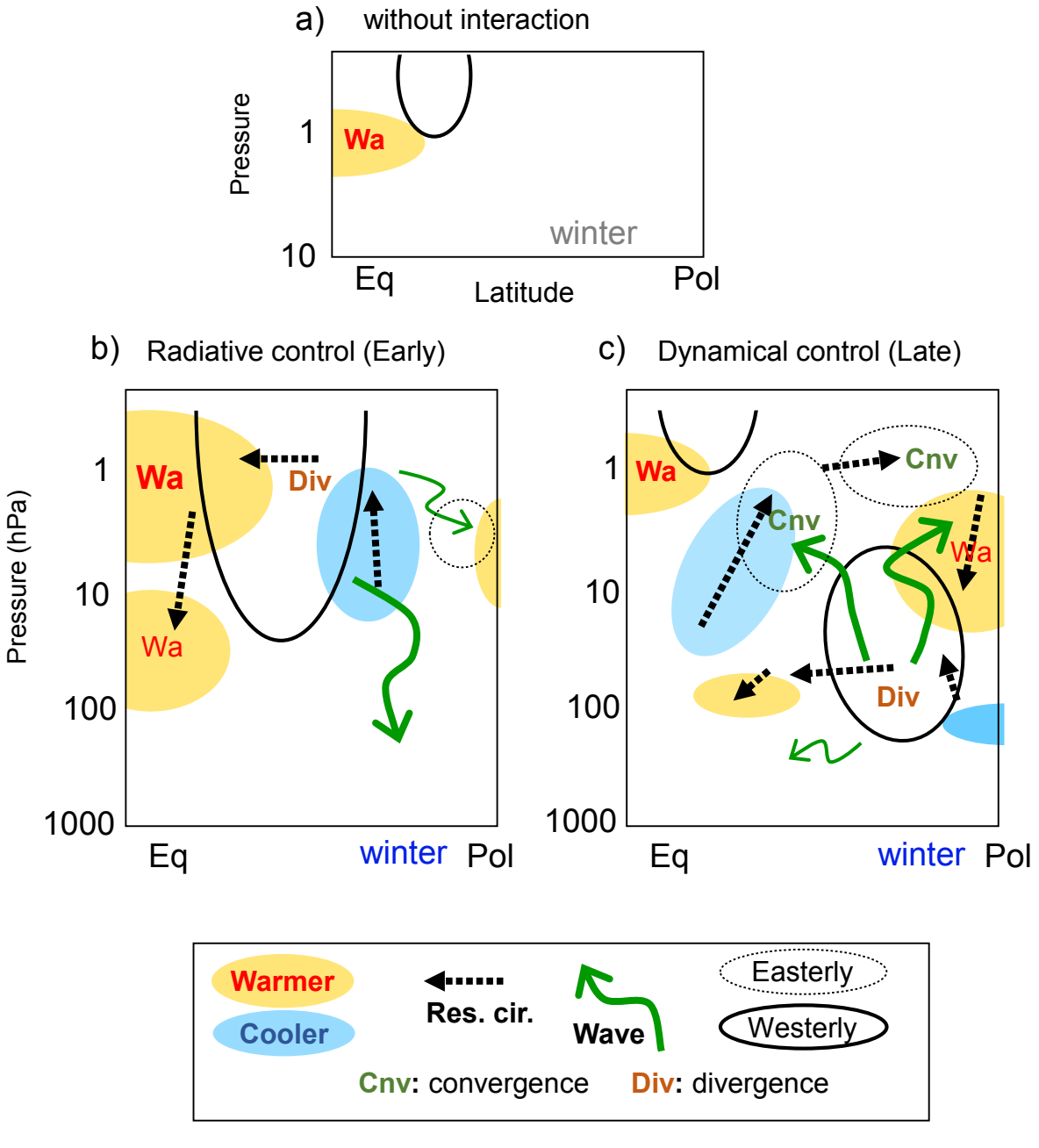
a) without interaction
Pressure
1
10
Wa
winter
Eq
Latitude
Pol
b) Radiative control (Early)
c) Dynamical control (Late)
Pressure (hPa)
1
10
100
1000
Wa
Div
Wa
Eq
winter
Pol
Wa
Cnv
Cnv
Wa
Div
Eq
winter
Pol
Warmer
Cooler
Res. cir.
Wave
Easterly
Westerly
Cnv: convergence
Div: divergence

Fig. 14

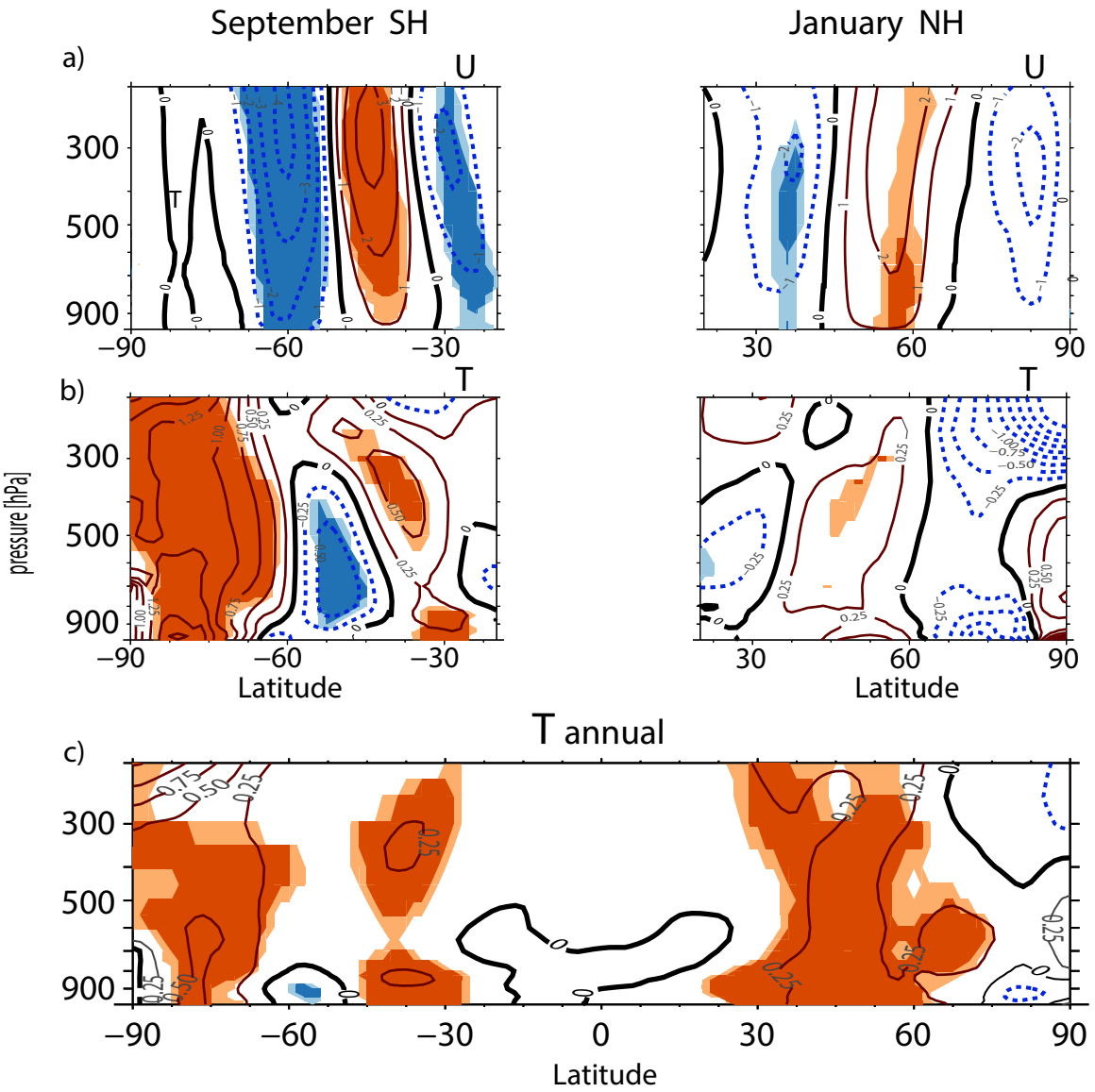
September SH
January NH
a)
U
T
300
500
900
−90
−60
−30
30
60
90
b)
pressure [hPa]
Latitude
T annual
c)
0
Latitude

Fig 15